ATTACHMENT A: CLASS VI PERMIT APPLICATION NARRATIVE
40 CFR 146.82(a)

Elk Hills A1-A2 Storage Project

Version	Submission Date	File Name	Description of Change
5	08/27/2025	Attachment A	Update for questions provided

Project Background and Contact Information

Carbon TerraVault 1 LLC (CTV), a wholly owned subsidiary of California Resources Corporation (CRC), proposes to construct and operate two CO_2 geologic sequestration wells at the Elk Hills Oil Field (EHOF) located in Kern County, California. This application was prepared in accordance with the U.S. Environmental Protection Agency's (EPA's) Class VI, in Title 40 of the Code of Federal Regulations (40 CFR 146.81). CTV is not requesting an injection depth waiver or aquifer exemption expansion.

CTV forecasts the potential CO_2 stored in the Monterey Formation at 0.25 - 0.75 million tonnes annually for 15 years with injection starting in 2025. The anthropogenic CO_2 will be sourced from either the Elk Hills 550 MW natural gas combined cycle power plant, renewable diesel refineries, and/or other sources in the EHOF area.

The EHOF storage site is 20 miles west of Bakersfield (Figure 1) in the San Joaquin Basin. The project will consist of two existing injectors, surface facilities, and monitoring wells. This supporting documentation applies to the two injection wells.

CTV has communicated project details and submitted regulatory documents to County and State agencies:

1. Kern County Planning and Natural Resource Development

   Director

   Lorelei Oviatt: (661)-862-8866

2. California Natural Resource Agency

   Deputy Secretary for Energy

   Matt Baker: (916) 653-5356

GSDT Submission - Project Background and Contact Information
GSDT Module: Project Information Tracking ***Tab(s):*** General Information tab; Facility Information and Owner/Operator Information tab Please use the checkbox(es) to verify the following information was submitted to the GSDT: ☒ Required project and facility details ***[40 CFR 146.82(a)(1)]***

Site Characterization

Regional Geology, Hydrogeology, and Local Structural Geology [40 CFR 146.82(a)(3)(vi)]

Elk Hills Field History

Discovered in the early 1900's the EHOF served as a Naval Petroleum Reserve (NPR-1) and was owned by the Navy and Department of Energy until its sale to Occidental Petroleum (Oxy) in 1998. In December 2014, Oxy spun off its California-specific assets including EHOF and the staff responsible for its development and operations to newly incorporated CRC. The Monterey Formation A1-A2 sequestration reservoir was discovered in the 1970's and has been developed with primary drilling and improved recovery with water and gas injection.

Elk Hills Geology Overview

The EHOF is located 20 miles west of Bakersfield in the fore-arc San Joaquin Basin (Figure 1). This continuously subsiding basin is a sediment filled depression that lies between the Sierra Nevada and Coast Ranges and is 450 miles long by 35 miles wide. The basin dates to the early Mesozoic (65 million years ago) when subduction was occurring off the coast of California. The plate tectonic configuration changed during the tertiary and the oceanic trench was transformed into the San Andreas fault, a zone of right-lateral strike-slip.

The Sierra Nevada, the most eastern province, is an immense section of granite that has been uplifted and tilted to the west. The Coast Ranges, which compose the western most province, are an anticlinorium in which the Mesozoic and Cenozoic sedimentary rocks are complexly folded and faulted. Between the Sierra Nevada and Coast Ranges is the San Joaquin Basin. When the basin first formed it was an inland sea between the two mountain ranges. Through time the Sierra Nevada volcanics and Coast Range sediments were eroded and filled the inland sea in what has become the San Joaquin Basin. This sediment included Monterey Formation turbidite sands that prograded across the deep floor of the southern basin.

Figure 1: Location of Elk Hills Oil Field, San Joaquin Basin, California.

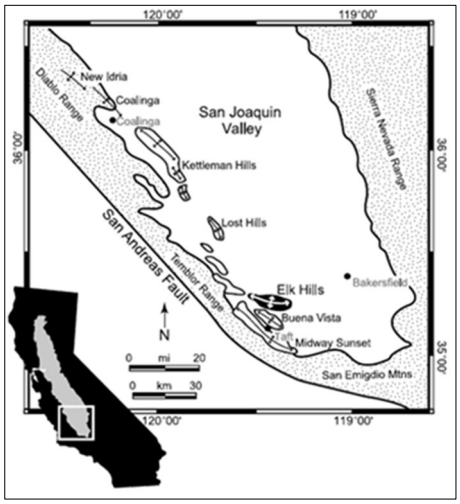

At the surface, the EHOF presents as a large WNW-ESE trending anticlinal structure, approximately 17 miles long and over seven miles wide. With increasing depth, the structure sub-divides into three distinct anticlines (Figure 2), separated at depth by inactive high-angle reverse faults. The anticlines formed in the middle Miocene and are associated with uplift due to southern basin shortening from the San Andreas Fault (Callaway and Rennie Jr., 1991).

Figure 2: The EHOF consists of the Northwest Stevens, 31S and 29R anticlines, with turbidite deposition occurring in fairways. The Monterey Formation A1-A2 CO_2 sequestration reservoir is located in the Northwest Stevens anticline (Zumberge, 2005).

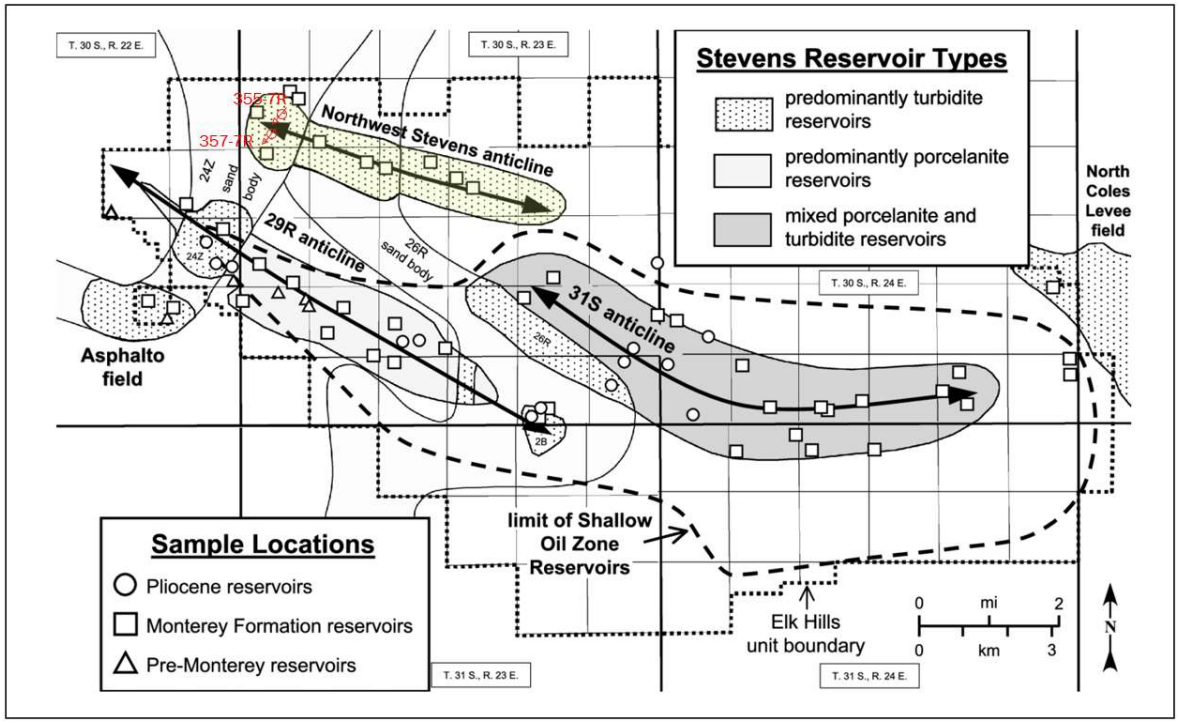

Geological Sequence

Figure 3 shows the stratigraphy of the EHOF. The two injection wells will inject CO_2 into the Miocene aged Monterey Formation A1-A2 at the Northwest Stevens anticline approximately 8,500 feet below the ground surface. This injection zone has a known reservoir capacity and injectivity as demonstrated by 40 years of oil and gas production and injection history.

Figure 3: Cross-section across the southern San Joaquin Basin showing the lateral continuity of the major formations (Zumberge, 2005). The storage reservoir for the project is the Monterey Formation and the confining shale is the overlying Reef Ridge Shale.

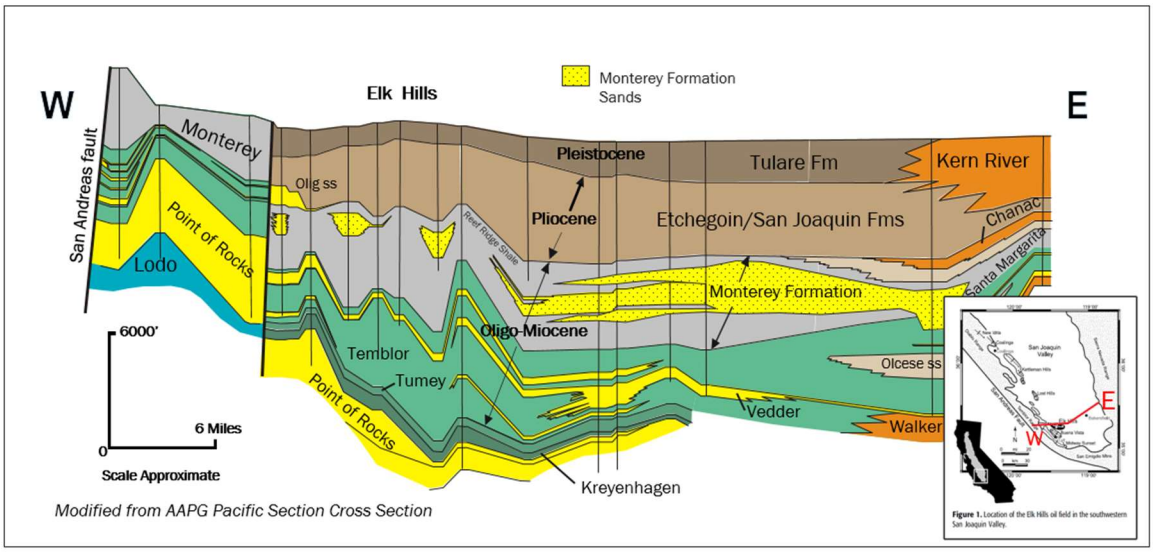

Following its deposition, Monterey Formation sands and shales were buried under more than 1,000 feet of impermeable silty and sandy shale of the confining Reef Ridge Shale. The Reef Ridge Shale is present over the southern San Joaquin Basin (Figure 4) and serves as the primary confining layer for the Monterey Formation A1-A2 reservoir with low permeability, sufficient thickness, and regional continuity well beyond the area of review (AoR). Above the Reef Ridge Shale are several alternating sand-shale sequences of the Pliocene Etchegoin Formation and San Joaquin Formations, and Pleistocene Tulare Formation. These formations are laterally continuous across the San Joaquin Basin as highlighted in Figure 3.

Figure 4: Reef Ridge Shale data coverage over the San Joaquin Basin (Hosford, 2007).

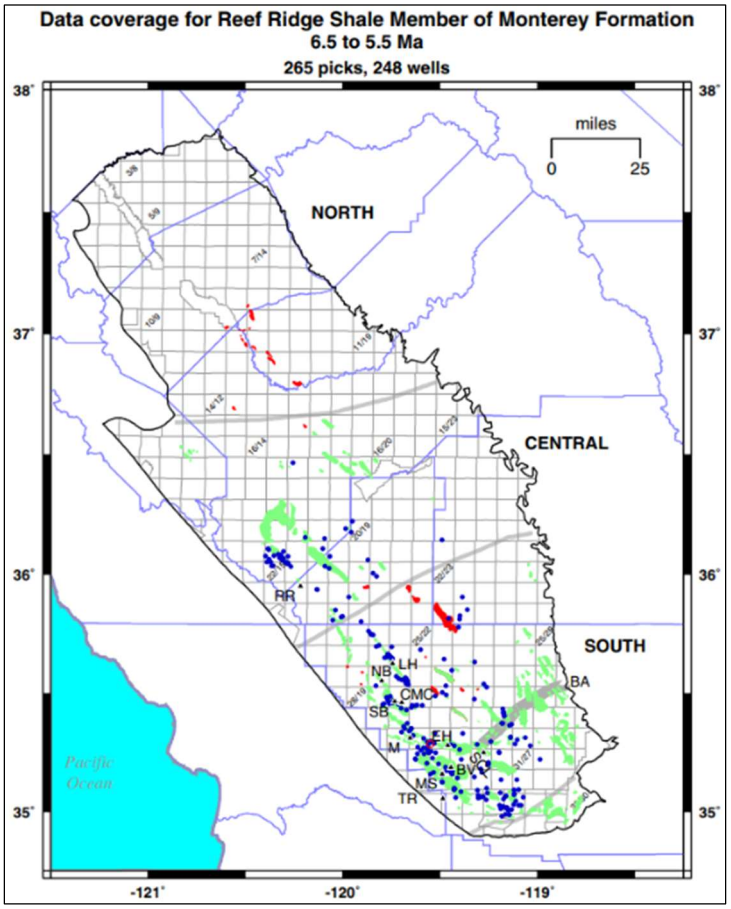

Maps and Cross Sections of the AoR [40 CFR 146.82(a)(2), 146.82(a)(3)(i)]

Elk Hills Data

To date, more than 7,500 wells have been drilled to various depths within the EHOF (Figure 5), creating an extensive library of information compiled within a comprehensive internal database. The database consists of core, electric and geophysical logs, and reservoir performance data such as production, injection, and pressures. In addition to well data, a 3-D seismic survey was acquired over the EHOF in 2000. Seismic combined with well data defines the sequestration zone, confining layers, and the subsurface structure.

Figure 5: Wells drilled in the EHOF that penetrate the confining Reef Ridge Shale. All wells shown have open-hole well logs that define structure and lithology of the storage reservoir and Reef Ridge confining layer. Wells with MICP core from the Monterey Formation are in purple.

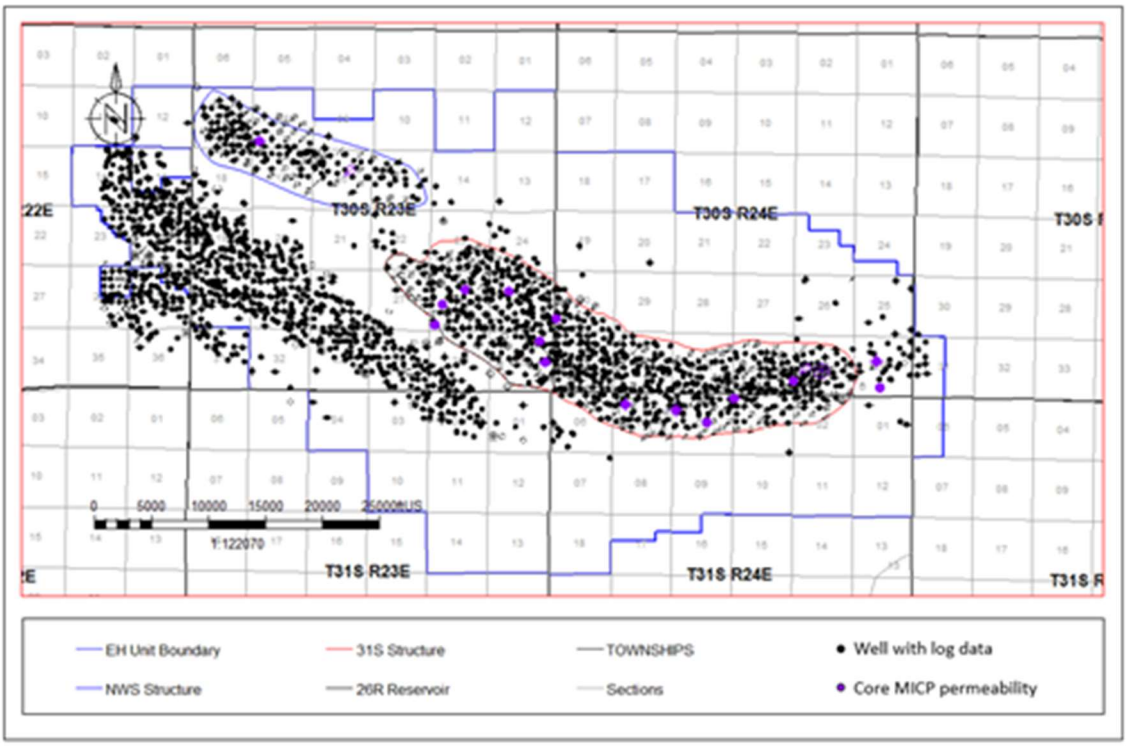

Elk Hills Stratigraphy

Major stratigraphic intervals include, from youngest to oldest, the Temblor Formation Reef Ridge Shale, Monterey Formation and Temblor Formation. This stratigraphy is shown in Figure 6 and discussed below. These formations are regionally continuous, with depositional environment affecting sand continuity and reservoir communication.

Figure 6: Cross section showing stratigraphy, type wells and the lateral continuity of major formations in the Northwest Stevens anticline.

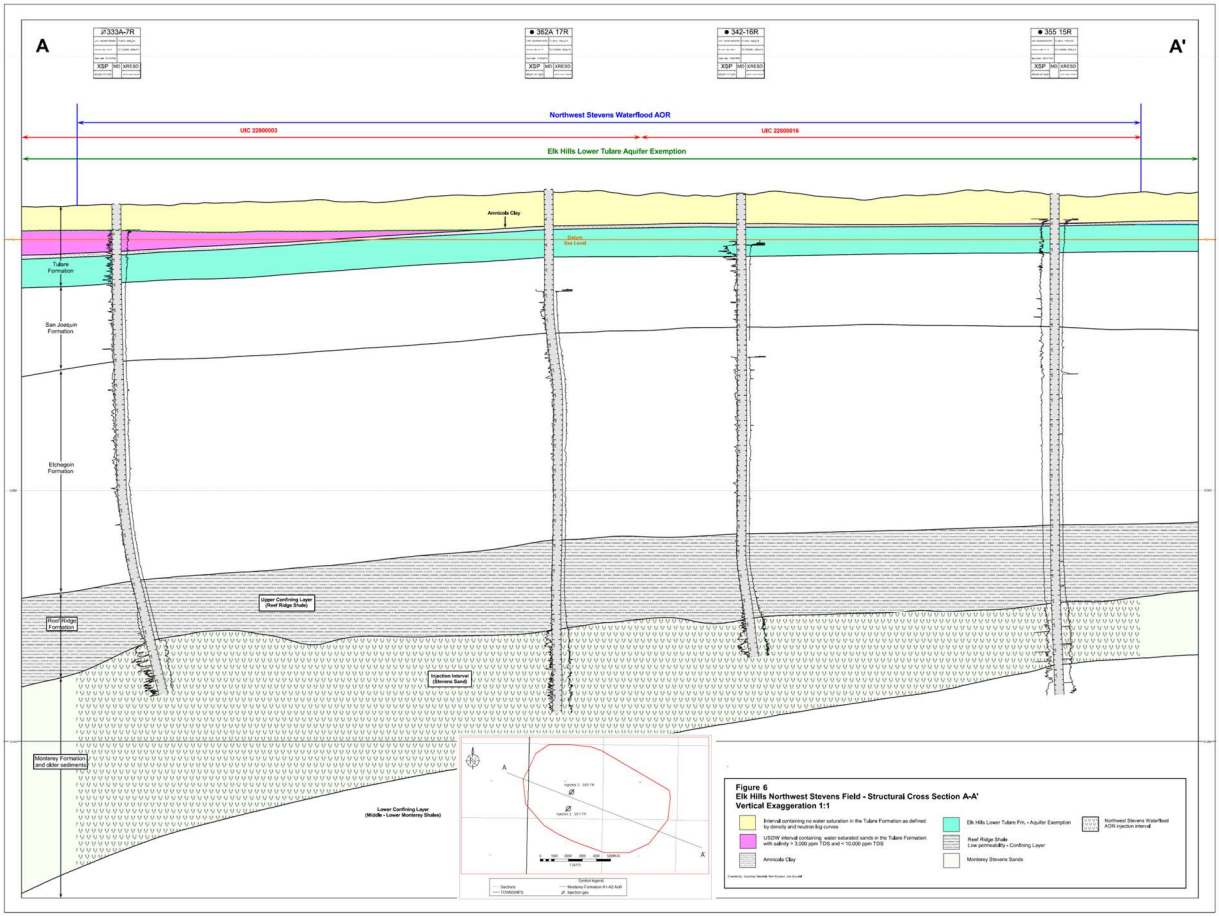

Tulare Formation

The Tulare Formation is a thick succession of nonmarine poorly consolidated sandstone, conglomerate, and claystone beds, which are exposed at intervals along the west border of the San Joaquin Valley. The Pleistocene aged Tulare Formation can be divided into the Upper Tulare and Lower Tulare members (Figure 7A), separated by a continuous low permeability claystone (Amnicola Clay). The sandstone beds have 34 - 40% porosity, 1,410 - 8,150 mD permeability, and are up to 50 feet thick, separated by much thinner beds of siltstone and claystone.

The conformable base of the Tulare represents a facies transition from Tulare Formation nonmarine fluvial and alluvial sediments to the shallow marine siltstones and shales of the San Joaquin Formation (Maher et al., 1975). The upper Tulare Formation outcrops at the EHOF and can be overlain by undifferentiated quaternary strata.

The Upper Tulare contains 3,000 - 10,000 milligrams per liter (mg/l) total dissolved solids (TDS) water and is the only USDW in the AoR. The Lower Tulare formation was approved as an exempt aquifer in 2018.

Figure 7A: The Tulare Formation consists of the Upper Tulare USDW and Lower Tulare and is separated by the Amnicola Clay. The Lower Tulare is an exempt aquifer. The Upper Tulare USDW has formation water 3,000 - 10,000 mg/l TDS.

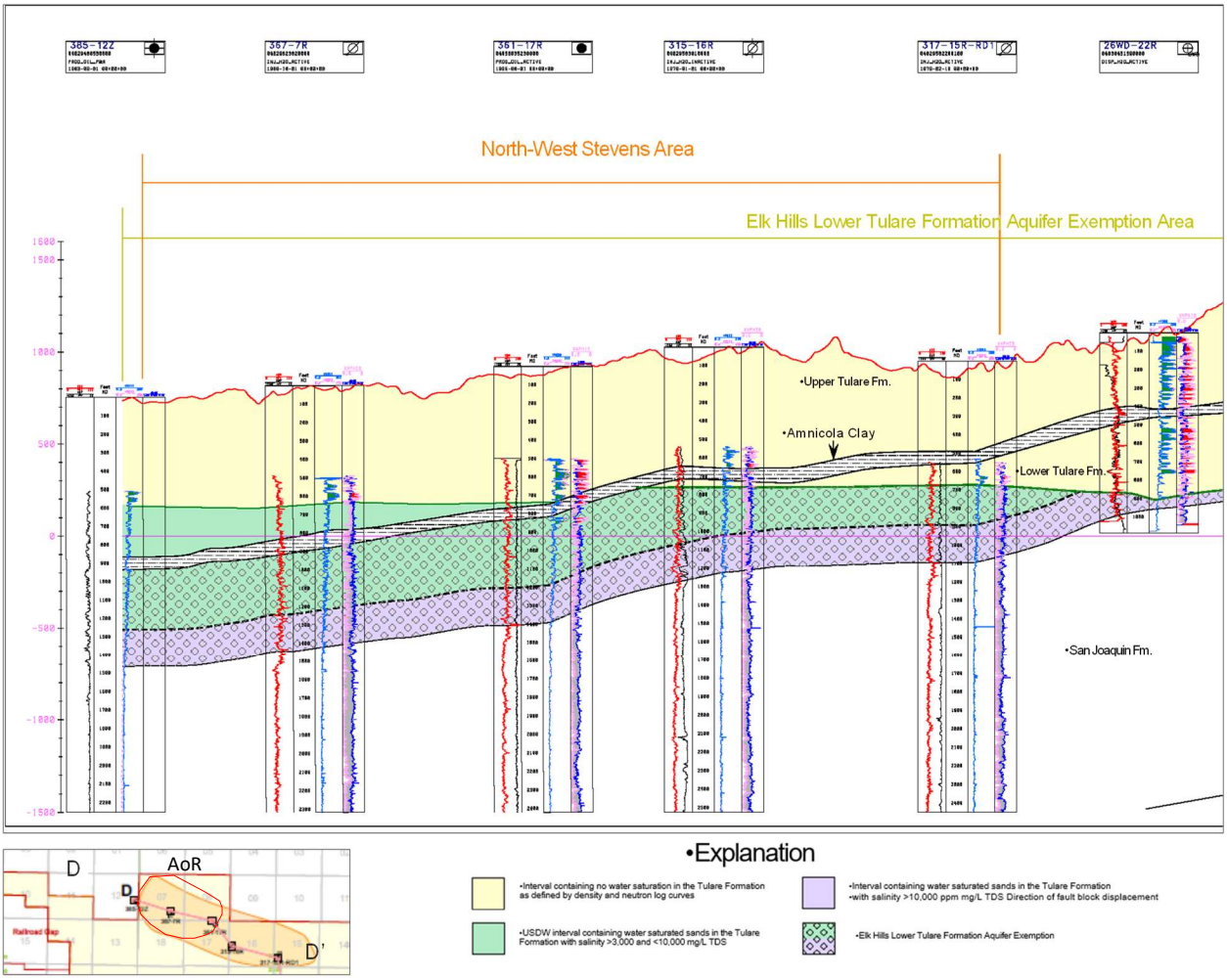

San Joaquin Formation

The upper portion of the San Joaquin Formation consists mostly of shale, interbedded clayey siltstone, and silty sandstone. The sandstone is scattered through the interval and is thin, very fine to fine grained sand and silt. The upper contact of the formation with the Tulare Formation is marked in most places by a pronounced lithologic change upward from shale to poorly sorted feldspathic sandstone and conglomerate. In some places the lower beds of sandstone and conglomerate of the Tulare Formation interfinger with the San Joaquin beds. The lower San Joaquin Formation conformably overlies the Etchegoin Formation and is comprised of

consolidated to semi-consolidated sandstone, siltstone, and shale of marine origin with 28 - 45% porosity and 64 - 6,810 millidarcy (mD) permeability.

The lower San Joaquin Formation contains the Mya Gas Sands, lenticular sand bodies that are charged with gas and are encased in claystone.

Etchegoin Formation

The marine deposited and Pliocene aged Etchegoin Formation is present in the subsurface across most of the southern San Joaquin Basin. At the EHOF, the formation is 1,500 - 4,000' in depth and consists of a lower silty shale member and an upper sandy interval (Maher, 1975). The sand dominated sequences consist of multiple sands that are 10 feet in thickness, 29 – 37% porosity, 32 – 826 mD permeability and can contain oil. Between sand reservoirs are laterally continuous shales, as shown in Figure 7B that are sealing and prevent hydraulic communication from above and below. Figure 6 shows a regional cross section, showing that the Etchegoin Formation is dominated by laterally continuous shales which limits hydraulic communication between sand lenses.

Figure 7B: Cross section showing lateral continuity of Etchegoin Formation sands and shales in the project area. The SP logs show sands shaded in yellow and shales shaded brown.

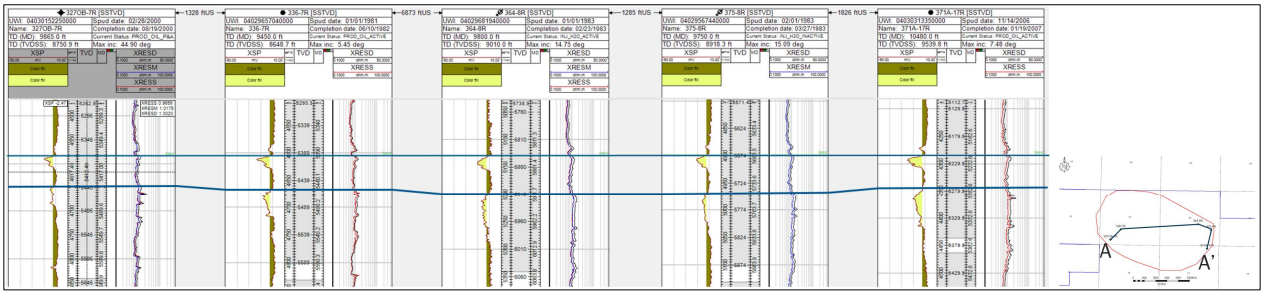

Reef Ridge Shale

Within the upper Miocene is the marine deposited siliceous Reef Ridge Shale, which is at 6,929-7,962 feet true vertical depth in the AoR. The Reef Ridge Shale is dominated by gray to grayish-black silty or sandy shale with rare silty and claybeds. At the EHOF the Reef Ridge Shale is continuous over the EHOF, ranges from 750 to 1,600 feet thick and has a permeability of less than 0.01 mD and 7% porosity.

The Reef Ridge directly overlies the Monterey Formation A1-A2 sequestration reservoir and has successfully contained oil and gas operations for over 40 years, and original oil and gas deposits for millions of years.

Monterey Formation

The Monterey Formation A1-A2 sequestration zone is approximately 8,500 feet deep and produces from turbidite sands. Turbidite deposited sands are interbedded with and bound above and below by siliceous shale. Sand porosity and permeability averages 16% and 60 mD, respectively.

The Monterey Formation A1-A2 sands were deposited in two coalescing turbidite channels which were influenced by the growing Elk Hills structure at the time of deposition. In Elk Hills the structure occurs synchronously with deposition. Although the Monterey Formation was deposited over the entire San Joaquin Basin, sands are sourced from the Sierra Nevada, San Emigdio and Coast Range highlands with deposition occurring in fairways (Figure 2). This depositional framework minimizes lateral communication of the Monterey Formation outside the EHOF. Figure 2 shows the orientation and depositional fairways for these channels in the Northwest Stevens anticline. The sands were largely aggregational with minimal erosive deposition. At the base of the Monterey Formation is the Lower Antelope Shale Member, a stack of thinly bedded siliceous shale with interbedded sands.

The reservoir is continuous across the AoR and sands pinch-out on the channel edges. The Monterey Formation A1-A2 sequestration reservoir has minimal connection outside the AoR, creating a reservoir with no connection to regional saline aquifers. Within the AoR there is no evidence of faults that transect the Monterey Formation or penetrate the Reef Ridge confining layer.

The Monterey Formation will be developed with the Elk Hills A1-A2 and the Elk Hills 26R reservoir projects. The AoR and injectors for each project are shown in Figure 8.

Figure 8: AoR and injection well location map for Elk Hills A1-A2 project. The injection wells, 355-7R and 357-7R are 1,250 feet apart. Also shown is the Elk Hills 26R AOR and injection wells.

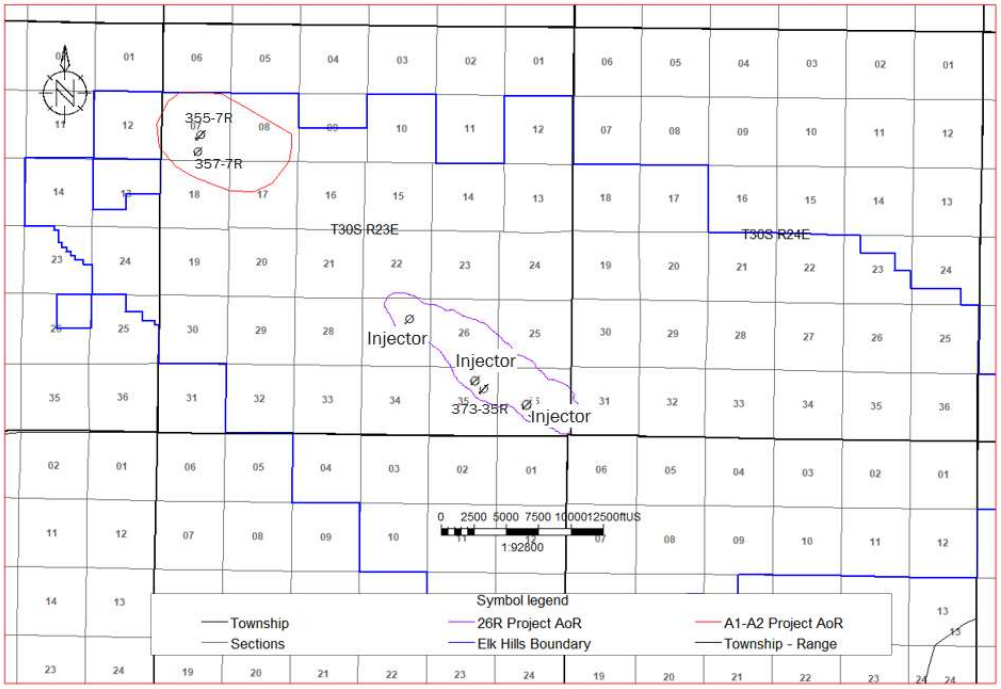

Underlying Monterey Formation A3+:

Underlying the Monterey A1-A2 Formation is the Monterey Formation A3+ reservoir. This stratigraphic package is not in communication with the A1-A2, as indicated by the following:

1. The two packages have been developed separately. The A1-A2 reservoir was previously pressure supported by gas injection (175 billion cubic feet injected) while the A3+ reservoir is currently pressure supported by waterflood (449 million barrels of water injected).
2. The Monterey Formation A1-A2 reservoir is at 200-300 psi and the A3+ reservoir is much higher at approximately 1,700 psi. This pressure differential is maintained due to hydraulic confinement between the two reservoirs. Pressure data obtained using Repeat Formation Testers (RFT) during the drilling of Oil & Gas wells in the project area has shown a clear separation in the pressure and pressure gradients in the A1-A2 reservoir in comparison to the A3+ reservoir. RFT data from two wells in the project area drilled in 2014 is shown below in Figure 10.
3. The laterally continuous A2 shale separates the reservoirs (Figure 9). This shale is greater than 20 feet thick across the AoR and prevents communication between the Monterey Formation A1-A2 reservoir and the Monterey Formation A3+ reservoir.

   The permeability function (Figure 19) is constrained with high clay content samples that enable the function to characterize the A2 shale permeability. Based on the 357-7R well, the A2 shale is 8900'-8920 feet in depth, 20 feet thick and has a permeability of 0.05 millidarcies. The derived permeability is shown in Figure 9.

Figure 9: 354X--7R showing the Monterey Formation A1-A2 reservoir and the laterally continuous A2 Shale above the Monterey Formation A3+ reservoir. The depths shown are for feet subsea true vertical depth and feet measured depth.

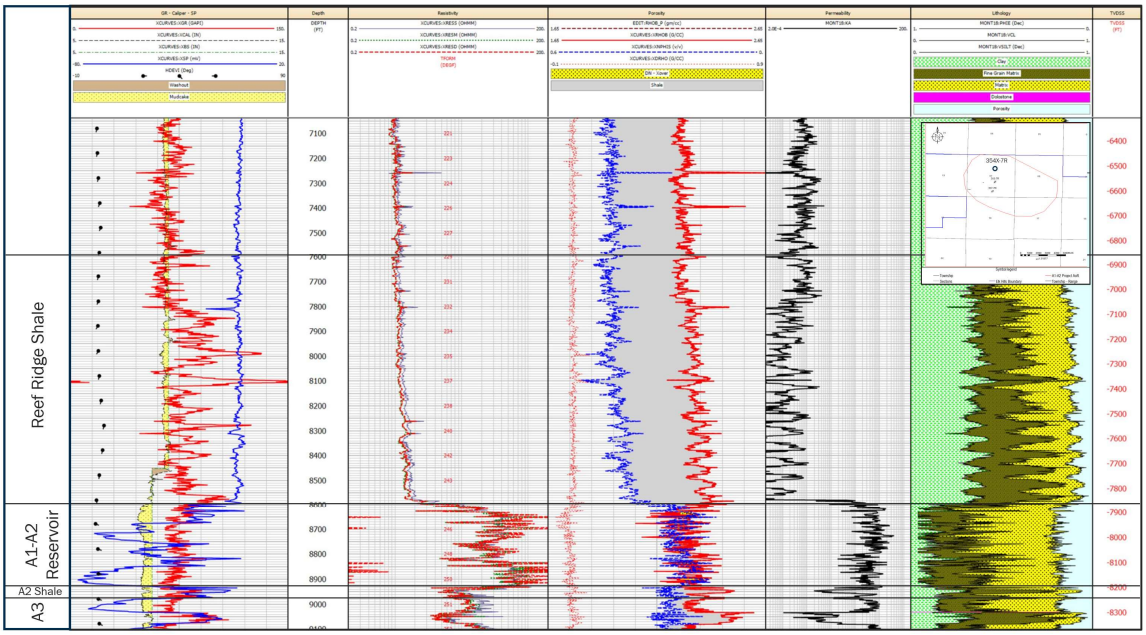

Figure 10: Repeat formation pressure data readings showing hydraulic separation between the A1-A2 and A3+ reservoirs. Large pressure difference between the two reservoirs and different fluid gradients as indicated by the red and blue dotted lines.

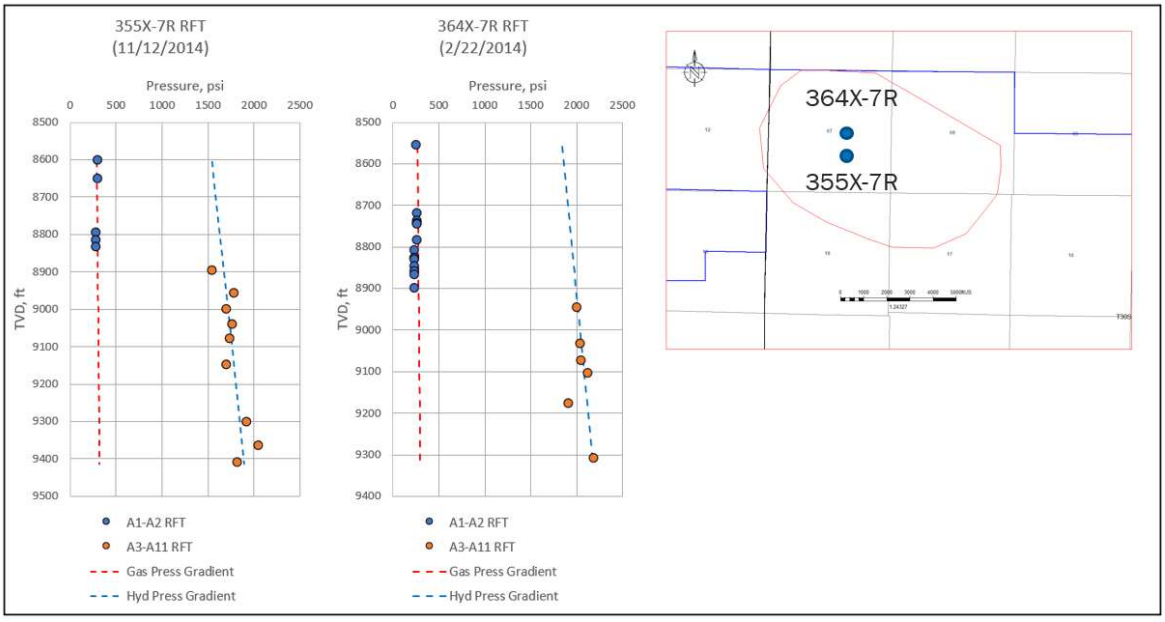

CTV will monitor the A3+ reservoir to confirm confinement of fluids between the A1-A2 and A3+ reservoirs. Details of the planned monitoring is provided in the Testing and Monitoring plan document. Summary:

The Northwest Stevens Monterey depositional framework and sand continuity have been established by static data that includes open-hole well logs and core as well as three dimensional seismic. Augmenting the static data is the dynamic data, which includes production, injection and pressure data gathered over the 40-year development history. The dynamic data, primarily pressure data (see Figure 10 Attachment A, and Figure 13, 14 Attachment B) gathered over the operational history of the reservoir, supports the geological interpretation that the A1-A2 is hydraulically separated from the underlying and overlying formations. The Gas production - Injection trends (see Figure 13, Attachment B) for the A1-A2 reservoir supports the geologic interpretation of sand continuity in the reservoir, with the responses seen in gas production with the start of injection in 1983 and cessation of injection in 2001.

Faults and Fractures [40 CFR 146.82(a)(3)(ii)]

Overview

The 31S and NWS anticlines formed bathymetric highpoints on the deep inland marine surface (seafloor), affecting geometry and lithology of the contemporaneously deposited turbidite sands and muds generated as subaqueous turbidite flows. Mid-Miocene thrust faults accompanying the development of the anticlines separate each structure at depth.

Initial interpretations of the three-dimensional (3D) seismic survey were based on a conventional pre-stack time migration volume. In 2019 the 3D seismic survey was re-processed using enhanced computing and statistics to generate a more robust velocity model. This updated processing to enhance the velocity model is referred to as tomography. The more accurate migration velocities used in the updated seismic volume allows a more focused structural image and clearer seismic reflections around tight folds and faults. The illustration in Figure 11 displays the location and extent of faults that helped to form the EHOF anticlines. Offsetting the NWS anticlines are high angle reverse faults that are oriented NW-SE. These inactive faults penetrate the lowest portions of the Monterey Formation but there is no data supporting transection of the Monterey Formation nor penetration into the lower Reef Ridge Shale.

Figure 11: EHOF Showing location of NWS and 31S anticlines with 3-D seismic boundary and line of cross sections. (Right) Cross Section A-A' and B-B' showing structure of EHOF anticlines with reverse faults.

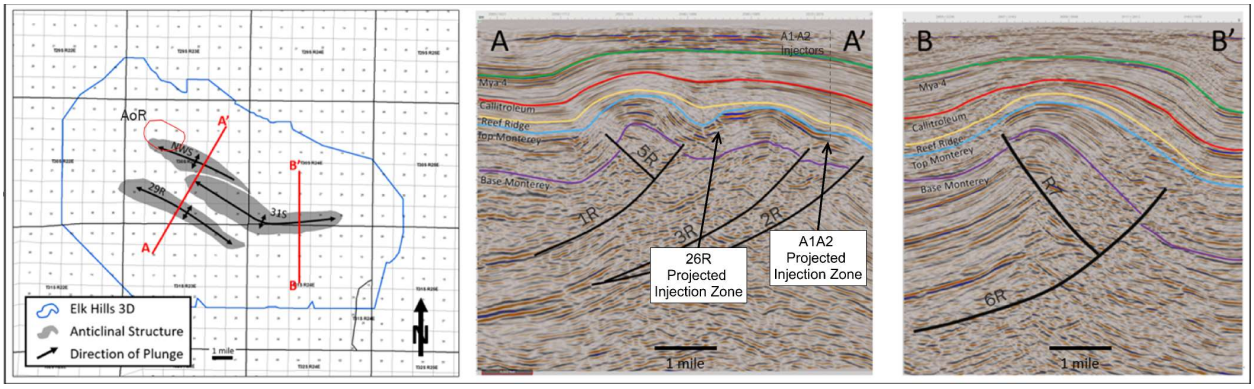

Fluid Confinement

Extensive well data, 3D seismic and operating experience, which includes the injection of water and gas, supports reservoir confinement of the CO_2 injectate in the Monterey Formation A1-A2 sands:

1. There are no faults that extend into the confining Reef Ridge Shale.
2. Extensive water and gas injection operations validate the reservoir characterization and demonstrate confinement within zones.
3. A pressure differential exists above and below the Reef Ridge confining interval, confirming lack of communication.
4. Geochemical analysis of reservoirs within the EHOF also confirms compartmentalization through several million years and effectiveness of the Reef Ridge Shale to contain the CO_2 injectate.

Seismic Control

The Reef Ridge is a thick continuous shale over the San Joaquin Basin. In the EHOF the thickness averages 1,555 feet (Figure 12) and is well resolved within seismic. Analysis of the three-dimensional seismic and well data provides no evidence that the faults either transect the Monterey Formation or penetrate the confining Reef Ridge Shale.

Figure 12: Reef Ridge Shale isochore map for the Elk Hills Oil Field.

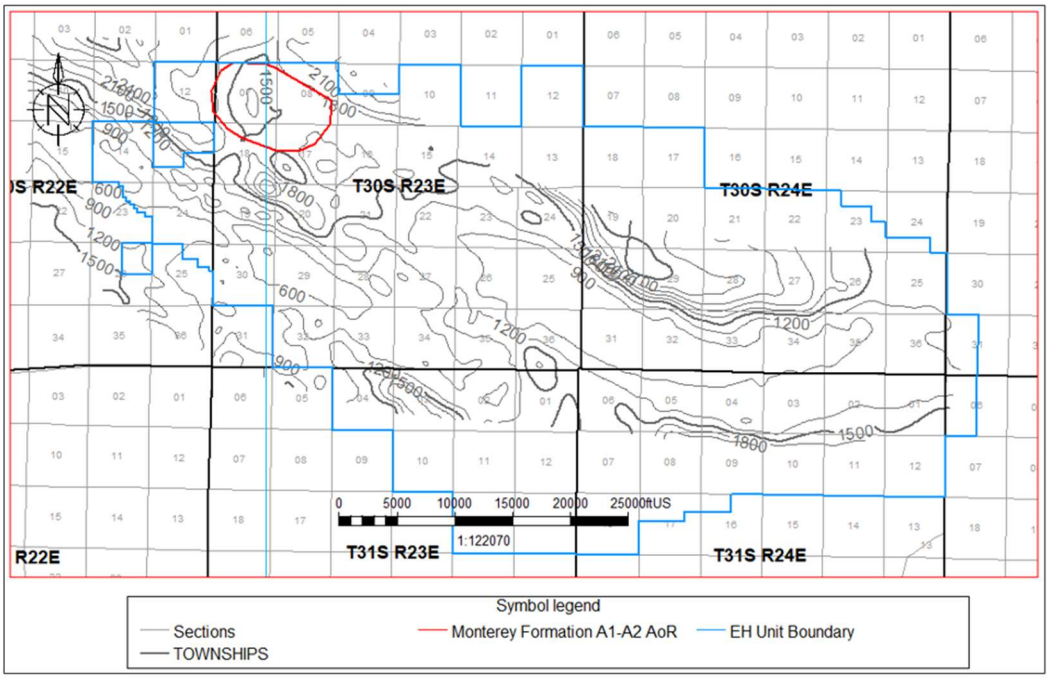

Waterflooding and Gas Injection

Waterflooding and gas injection for the purpose of pressure support is conducted under a set of Class II UIC permits issued by CalGEM and reviewed by the State Water Resources Control Board. To date, more than five million barrels of water and 175 billion cubic feet of gas have been injected into the Monterey Formation A1-A2 sands. There has been no evidence of water or gas migrating out of the reservoir or through the Reef Ridge Shale. Historic waterflood and gas injection results provide clear evidence that the planned sequestration zone is vertically and aerially confined.

Pressure Differentials

The Monterey Formation A1-A2 sequestration zone average current pressure is approximately 230 psi. Overlying the sequestration zone, and separated by the confining Reef Ridge Shale, the Etchegoin Formation aquifer sands are at a much higher pressure of 1,500 psi (0.43 psi/ft gradient at 3,600 feet depth). This pressure differential of 1,300 psi between the overlying Etchegoin Formation and Monterey Formation is maintained because the Reef Ridge is sealing and there are no transmissive features. Figure 13 shows an example of RFT pressure data collected in 2004 during the drilling of an Oil & Gas well near the project area. The RFT data shows that the Etchegoin is hydraulically separated from the deeper Monterey formation and at a much higher pressure.

Figure 13: Etchegoin and Monterey RFT data collected during the drilling of Oil & Gas well 321X-16R near the project area showing hydraulic separation between the two formations.

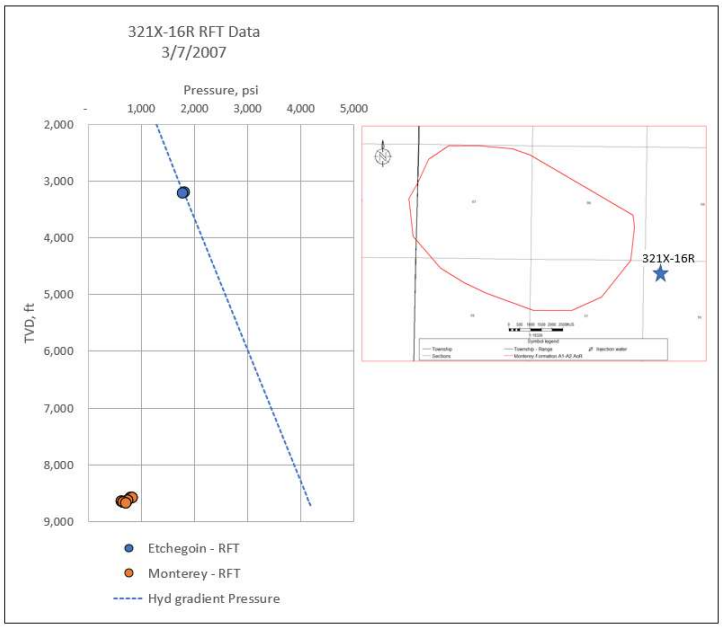

Geochemical Analysis

Geochemical data from 66 oil samples also confirms there is vertical isolation between the Monterey Formation and the overlying formations (Zumberge, 2005). Analysis revealed five distinct oil families (Figure 14) sourced from the Miocene Monterey Formation and tied to stratigraphic intervals (sample locations shown on Figure 2). The differences between the distinct geochemical compositions of the Monterey Formation and overlying formations hydrocarbons suggests "minimal up-section, [and] cross stratigraphic migration". The authors conclude that the hydrocarbons present in the overlying formations are from "another Monterey source facies (perhaps the youngest) with charging of Pliocene reservoirs" and not the result of upward movement from the older Miocene reservoirs.

The geochemical oil family data conclusions are supported by the pressure data (Figure 13) showing that formations are not in communication due to reservoir depletion.

Figure 14: Elk Hills oil families (Zumberge, 2005).

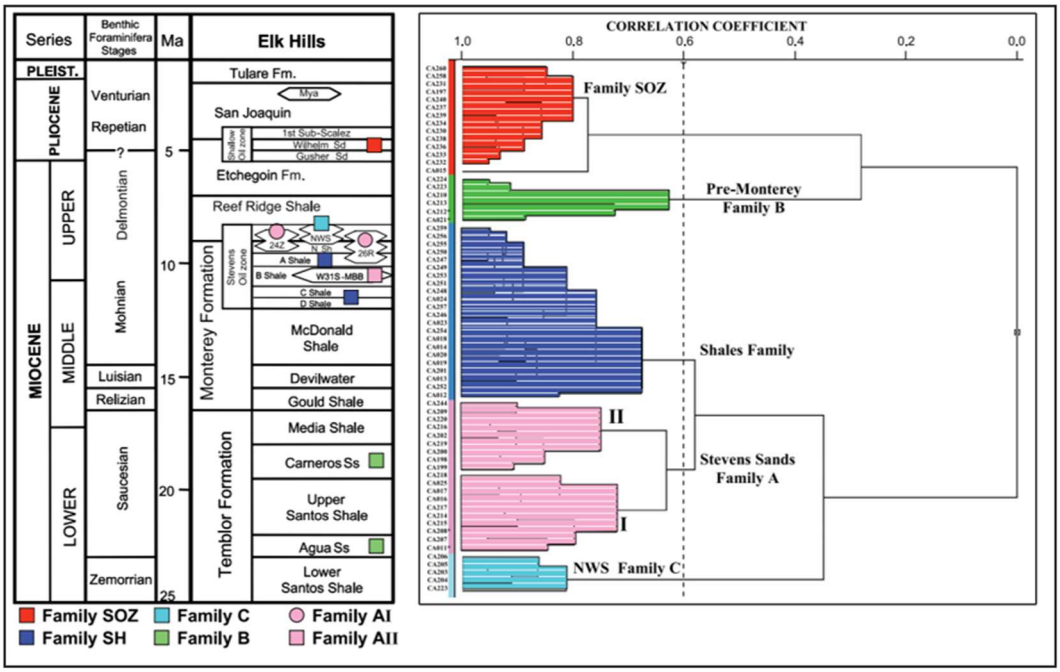

Injection and Confining Zone Details [40 CFR 146.82(a)(3)(iii)]

Depth and Thickness

Depths and thickness of the Monterey Formation A1-A2 reservoir and Reef Ridge Confining Shale (Table 1) are determined by structural and isopach maps (Figure 15) based on well data (wireline logs). Variability of the thickness and depth measurements is due to:

1. Reef Ridge and Monterey Formation structural variability due to the Elk Hills anticlinal structure.
2. Reef Ridge Shale thickness variability due to deposition of the Monterey Formation sands. In the AoR, the Reef Ridge Shale minimum thickness corresponds to a high in Monterey Formation A1-A2 sand thickness.
3. Monterey Formation A1-A2 thickness variability is from pinch-out of the reservoir on the structure.

Table 1: Reef Ridge Shale and Monterey Formation A1-A2 thickness and depth for the AoR.

Zone	Property	Low	High	Mean
Confining Zone Reef Ridge Shale	Thickness (feet)	1,122	1,892	1,555
	Depth (feet TVD)	6,929	7,962	7,441
Reservoir Monterey Formation A1-A2 Sand	Thickness (feet)	27	548	204
	Depth (feet TVD)	8,403	9,598	8,907

Figure 15: Reef Ridge Shale and Monterey Formation A1-A2 thickness and depth maps.

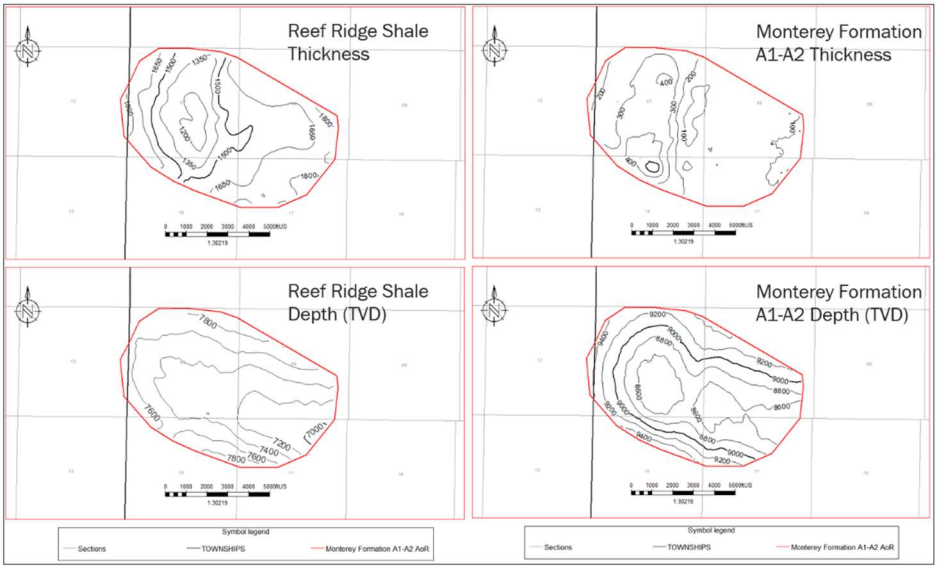

Variability in the thickness and depth of the either the Reef Ridge Shale or the Monterey Formation A1-A2 sands will not impact confinement. CTV will utilize thickness and depths shown when determining operating parameters and assessing project geomechanics.

Facies Changes in the Injection or Confining Zone

The Monterey Formation A1-A2 reservoir and Reef Ridge Shale has been defined with extensive data (Figure 16), with a total of 255 well and spacing of 400-800 feet. Each of these wells is used to define stratigraphy, lithology/facies and reservoir properties for the static geological model and the maps shown in Figure 15. This quantity and spacing of data is more than sufficient to generate a data driven static model that define facies changes in for the reservoir and confining zone.

For example, during the drilling of well 355-7R in 1972 spontaneous potential (SP) resistivity (dual induction laterlog), density, neutron porosity and formation dip from 10,509' to 3,393', covering the Etchegoin, Reef Ridge Shale confining layer and the Monterey Formation A1-A2 storage reservoir. In addition, 28 sidewall core samples were obtained over the same interval (no detailed analysis of the core samples). The log data supports the characterization of the injection zone and the confining zone at the well site.

Based on Monterey Formation A1-A2 operational experience and plume modeling results, there are no facies changes that will either impact injection operations or confinement.

Figure 16: Well data used to define the Monterey Formation A1-A2 injection reservoir and confining zone. These wells have open-hole log data that is used to establish, clay volume, porosity, permeability, and facies (sand and shale) that are used in the static geological model.

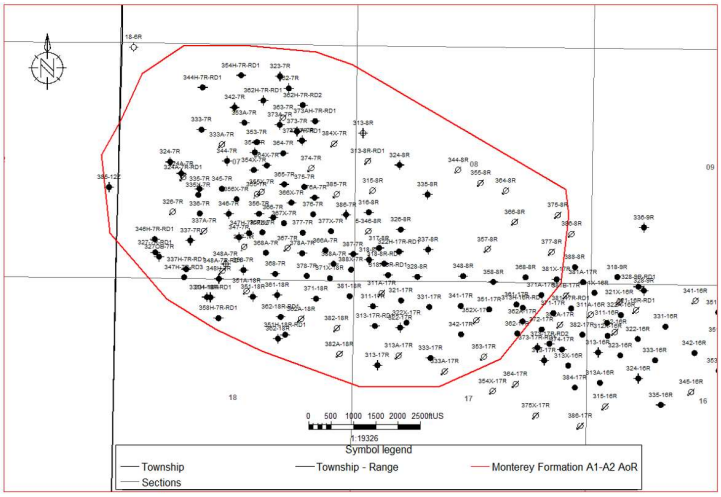

Mineralogy

Monterey Formation A1-A2:

X-ray diffraction data has been compiled and compared from 9 wells with a total of 108 data points. Clay speciation has been found to be consistent throughout the AoR. Offset well 367-7R (Figure 17) provides an example of the mineralogy for the reservoir interval in 357-7R. Clean reservoir sand intervals have an average of 43% quartz, 38% potassium feldspar, albite and oligoclase as well as 7% total clay.

Figure 17: Monterey Formation A1-A2 sand mineralogy from well 367-7R. The map shows the location for 367-7R and the other wells with XRD in the Elk Hills field.

DEPTH	GDI	SAMP/ WT	QTZ	CHRT	OP-A	OP-CT	ALB	OLIG	AND	KSPAR	CALC	DOLO	PYR	KAOL	CHLOR	ILL/SMEC
8551.9	2.62	8.34	30	13	0	0	17	0	2	21	2	0	1	0	0	14
8552	2.62	9.41	29	13	0	0	14	10	0	15	3	0	0	0	3	14
8554.1	2.62	10.73	45	0	0	0	19	0	2	20	4	0	0	0	0	10
8560.6	2.62	11.37	44	0	0	0	15	11	0	17	5	0	0	2	0	6
8570	2.62	8.32	33	0	0	0	17	8	4	17	3	0	0	0	0	8
8583	2.6	14.88	45	0	0	0	15	11	0	18	4	0	0	0	0	7
8604.3	2.6	18.83	21	21	0	0	15	0	10	14	2	0	0	0	0	17
8634.3	2.52	12.65	44	0	0	0	14	13	1	17	3	0	0	0	0	6
8648.6	2.52	14.16	47	0	0	0	14	3	5	19	3	0	0	0	0	5
8649.2	2.42	15.58	49	0	0	0	18	0	4	14	3	0	0	2	0	6
8649.8	2.42	8.76	50	0	0	0	17	0	4	17	1	2	0	3	0	6
8660.9	2.42	11.24	45	0	0	0	14	9	4	17	2	1	0	2	0	6
8651.4	2.42	8.75	45	0	0	0	14	0	4	19	3	0	0	0	0	10
8656	2.43	23.41	38	0	0	0	14	10	4	14	12	2	0	0	0	6
8702.5	2.41	10.58	40	13	0	0	15	0	5	18	2	0	0	0	0	7

GDI = Grain Density
Sample WT = Weight of Fresh Sample Crushed For Analysis
QTZ = Quartz
CHRT = Chert
OP-A = Opal-A
OP-CT = Opal-CT
ALB = Albite
OLIG = Oligoclase
AND = Andesine
KSPAR = Potassium Feldspar
CALC = Calcite
DOLO = Dolomite
PYR = Pyrite
CHLOR = Chlorite
Ill/SMEC = Illite - Smectite

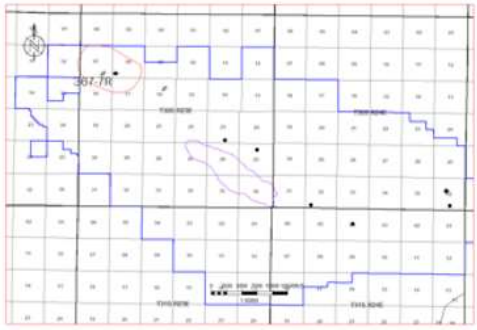

Reef Ridge Shale:

Mineralogy data is available from 241 samples from ten wells within the boundary of the EHOF (Figure 18). Samples were analyzed using both Fourier Transform Infrared Spectroscopy (FTIR) and x-ray diffraction (XRD) (see Appendix: Core Data).

Clay minerals comprise approximately 25-30% of the bulk rock mineralogy for the non-carbonate rich samples. Clay speciation is dominated by mixed layer illite/smectite, comprising 65% of the clay minerals, with kaolinite as the second most dominant clay species at 27% of the clay minerals. Of the non-clay mineralogy, quartz, feldspar, and biosiliceous quartz are the primary constituents. Opal CT, chert, quartz, and feldspars comprise approximately 70% of the non-clay rock mass. The

remainder of the rock is primarily cristobalite. Of the 241 total samples, only 17 (7% of the total count) were considered "carbonate rich" with a total carbonate weight percent greater than 30%.

While these wells are not located in the AoR, they are representative of the marine Reef Ridge Shale in the AOR due to the depositional continuity of the unit, proximity to the project and consistency of facies and properties.

Figure 18: Map showing the location of wells with Reef Ridge Confining Zone core data.

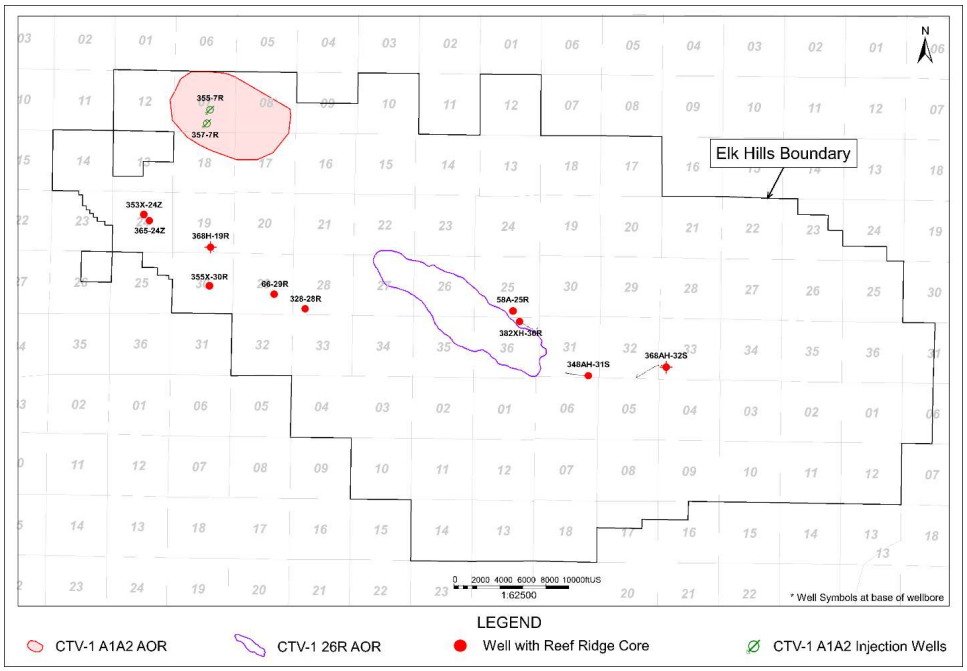

Porosity and Permeability

Monterey Formation A1-A2:

Wireline log data was acquired with measurements that include but are not limited to spontaneous potential, natural gamma ray, borehole caliper, resistivity as well as neutron porosity and bulk density.

Formation porosity is determined from bulk density using 2.65 g/cc matrix density as calibrated from core grain density and porosity data.

Volume of clay is determined by neutron-density separation and is calibrated to core data.

Log-derived permeability is determined by applying a core-based transform that utilizes mercury injection capillary pressure porosity and permeability along with clay values from x-ray diffraction or Fourier transform infrared spectroscopy. Core data from 13 wells (Figure 19) with 175 (see Appendix: Core Data) data points were used to calibrate log porosity and to develop a permeability transform. This distribution of wells and data points covers Monterey Formation sands in the Elk Hills field and ensures coverage of the porosity-permeability range in the storage reservoir. An example of the transform from core data is illustrated in Figure 19 below.

Figure 19: Permeability function developed based on mercury injection capillary pressure data and calculated from log derived porosity and clay volume. Map shows the locations for wells with Monterey Formation sand core data used in the function.

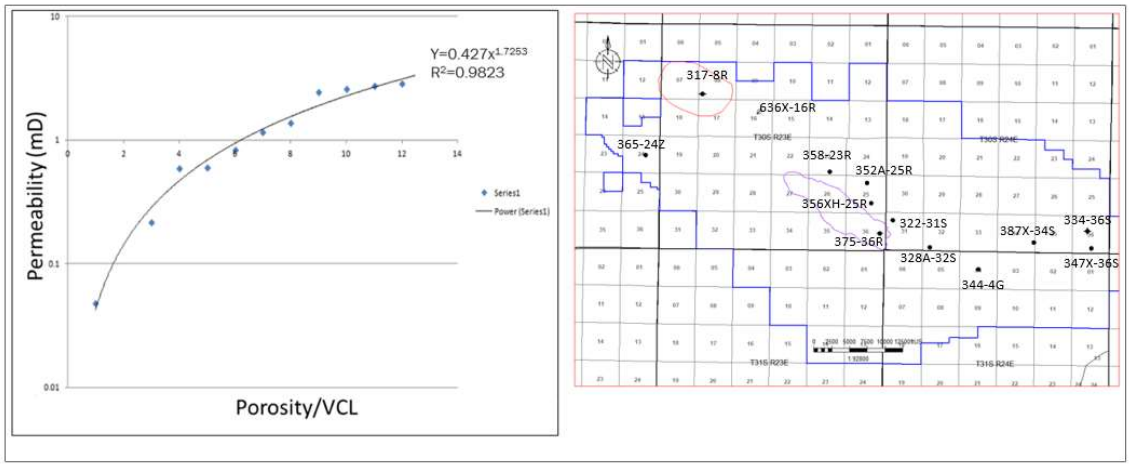

In the example below for the Monterey Formation A1-A2 sands, the porosity ranges from 11% - 27% with a mean of 21%. The permeability ranges from 0.1 mD - 1300 mD with a log mean of 108 mD (Figure 20).

Figure 20: Porosity and permeability for well 357-7R, showing the distribution and the input and output log curves. Lithology and clay volume (VCL) was calculated using the neutron-density log separation and gamma ray. Sands have less neutron-density separation compared to silts and shale.

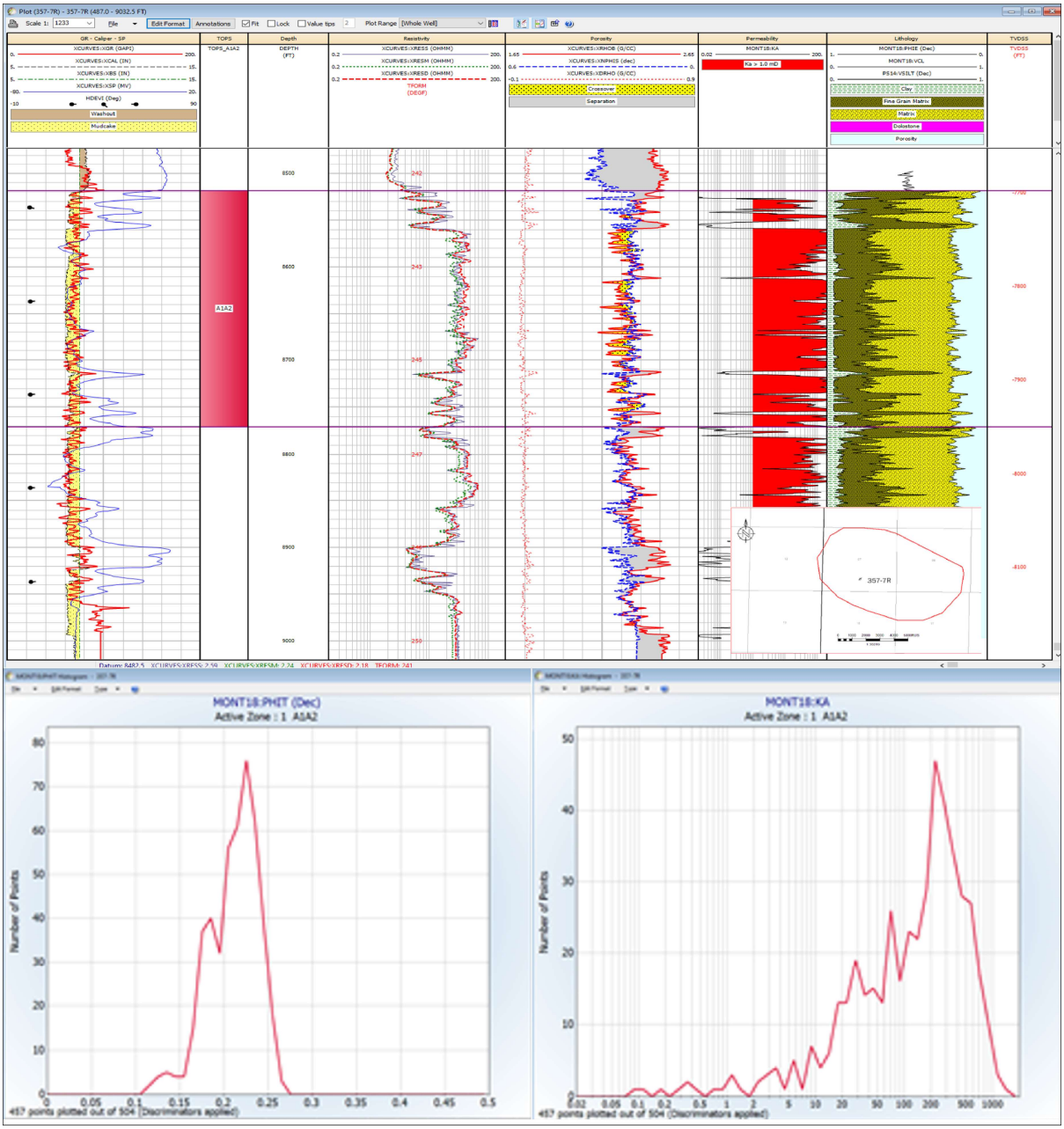

Reef Ridge Shale:

The average porosity of the Reef Ridge is 14.9% based on 40 mercury injection capillary pressure (MICP) core data points (see Appendix: Core Data).

The geometric mean permeability of the Reef Ridge is 0.00083mD based on 40 MICP core data points from six wells (see Appendix: Core Data). See Figure 18 for location of the wells with MICP data.

Using log data for the Reef Ridge in the project area, average porosity and permeability were calculated on 23 wells (Table 2). The arithmetic mean of the log derived porosity is 13.4% and the geometric mean of the log derived permeability is 0.0012 mD, which corroborates that the Reef Ridge is a low permeability cap rock.

Table 2: Permeability and porosity for the Reef Ridge Shale from log data in 23 wells.

Well	Average Porosity (%)	Geometric Mean Permeability (mD)
311A-17R	14.2%	0.0044
313-8R-RD1	14.8%	0.0028
321-17R	13.1%	0.0004
324A-7R-RD1	12.1%	0.0001
335-8R	7.5%	8.06E-06
335X-7R	11.7%	0.0007
341-17R	11.2%	0.0002
353A-7R	16.2%	0.0084
354X-7R	15.9%	0.0014
355-8R	9.0%	2.23E-05
356X-7R	14.3%	0.0033
357-7R	10.7%	0.0003
358-8R	14.4%	0.0028
361-17R	15.7%	0.0061
362A-17R	14.3%	0.0026
363-7R	14.2%	0.0029
366-7R	11.9%	0.0006
371A-17R	13.8%	0.001
371X-18R	11.4%	0.0002
376A-7R	16.3%	0.0101
377-7R	13.7%	0.0014
377X-7R	12.2%	0.0005
388A-7R	12.8%	0.0022
All Wells	**13.4%**	**0.0012**

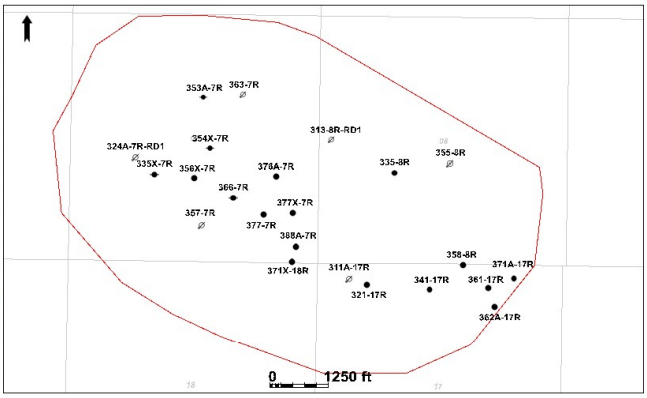

Reef Ridge Shale Capillary Pressure:

Capillary pressure is the difference across the interface of two immiscible fluids. Capillary entry pressure is the minimum pressure required for an injected phase to overcome capillary and interfacial forces and enter the pore space containing the wetting phase.

The capillary pressure of the Reef Ridge confining zone is 4,220 psi in a CO_2-brine system based on 39 mercury injection capillary pressure (MICP) core data points from six wells (Figure 21). The capillary pressure was determined by applying CO_2-brine corrections to air-mercury test data. An interfacial tension of 480 dynes/cm was used for air-mercury and 30 dynes/cm was used to convert to CO_2-brine. The cosine of contact angles of 0.766 and 0.866 degrees were also used for air-mercury and CO_2-brine, respectively.

Figure 21: Capillary pressure versus wetting phase saturation for core data from six wells.

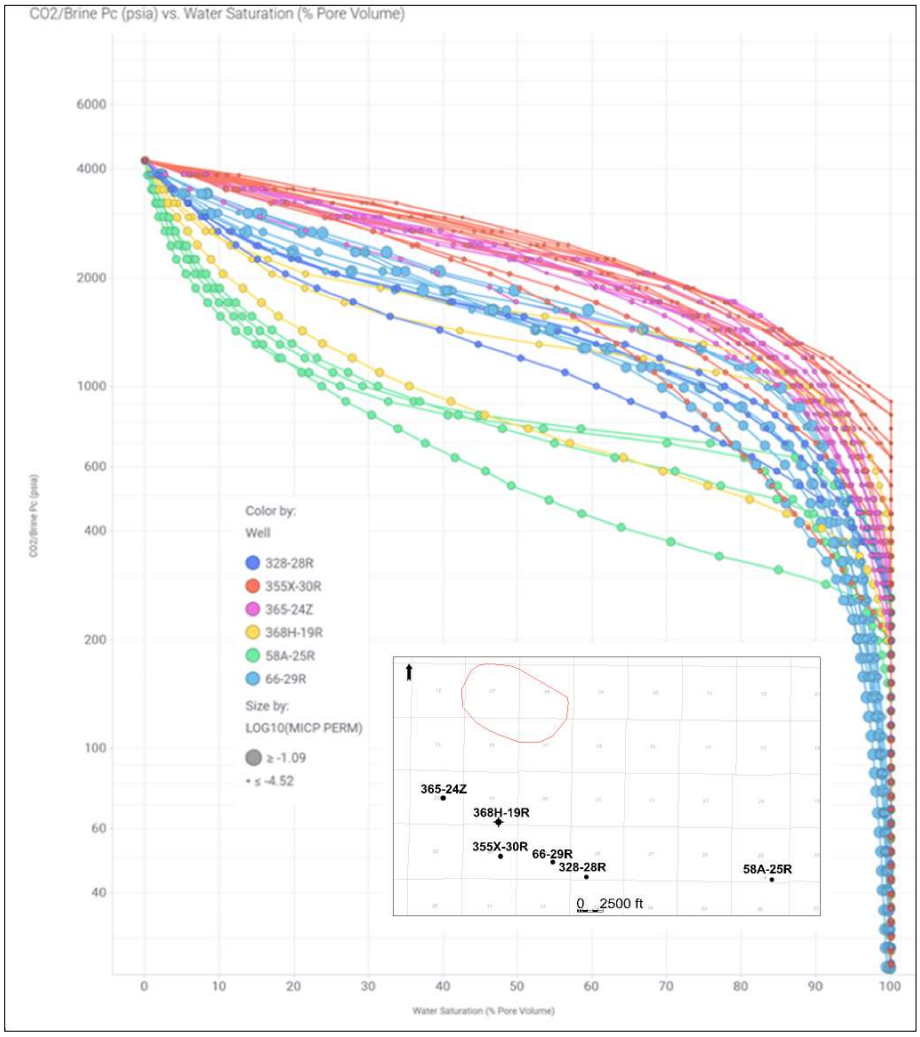

Geomechanical and Petrophysical Information [40 CFR 146.82(a)(3)(iv)]

Reef Ridge Ductility:

Over 40 years of water and gas injection have been confined by the shale in AoR and the San Joaquin Basin. Ductility and the unconfined compressive strength (UCS) of the Reef Ridge Shale are two properties used to describe geomechanical behavior. Ductility refers to how much the Reef Ridge Shale can be distorted before it fractures, while the UCS is a reference to the resistance of the Reef Ridge to distortion or fracture. Ductility decreases as compressive strength increases. Within the AoR, 18 wells had compressional sonic data over the Reef Ridge Shale to calculate ductility and UCS, comprising 59,214 individual logging data points. The location for the 18 wells is shown on the map in Figure 22.

Ductility and rock strength calculations were performed based on the methodology and equations from Ingram & Urai, 1999 and Ingram et. al., 1997. Brittleness is determined by comparing the log derived unconfined compressive strength (UCS) vs. an empirically derived UCS for a normally consolidated rock (UCS_{NC}).

$$UCS_{NC} = 0.5\sigma'$$

$$\sigma' = OB_{Pres} - P_P$$

$$BRI = \frac{UCS}{UCS_{NC}}$$

An example calculation for the well 354X-7R is shown below (Figure 22). UCS_CCS_VP is the UCS based on the compressional velocity, MECPRO:UCS_NC is the UCS for a normally consolidated rock, and MECPRO:BRI is the calculated brittleness using this method. Ductility less than two is shaded red.

Figure 22: Unconfined compressive strength and ductility calculations for well 354X-7R. The Reef Ridge Shale ductility is less than two (red shaded region in last track).

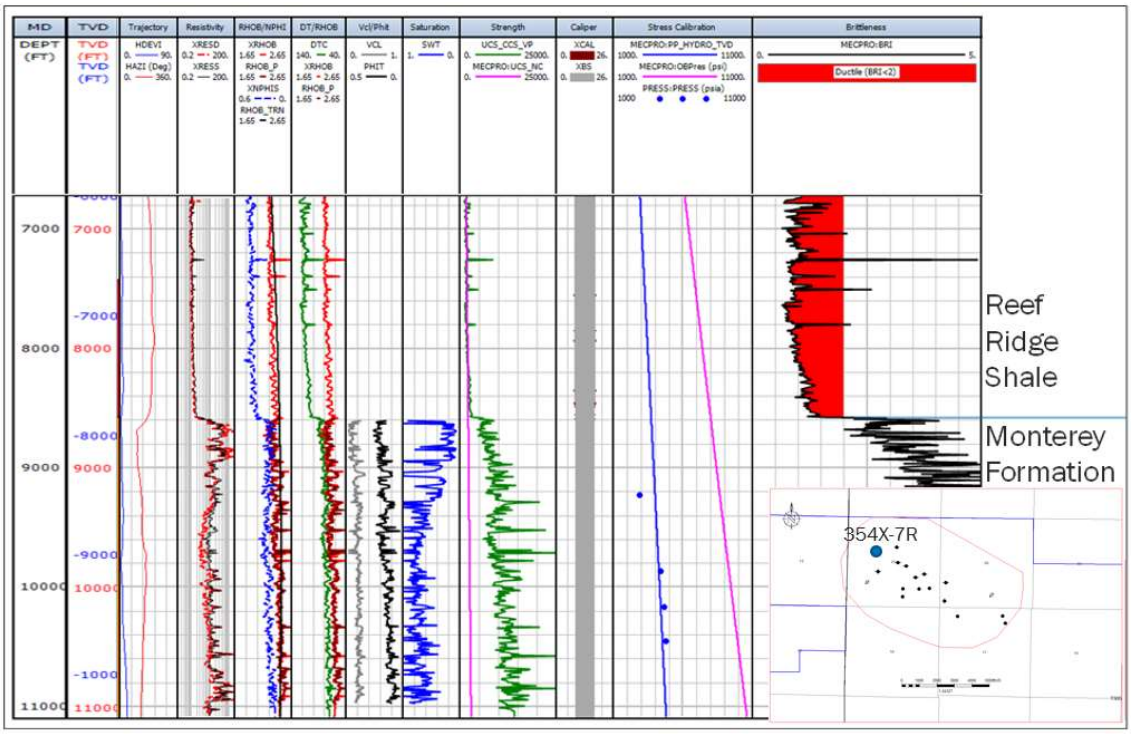

At the Reef Ridge Shale and Monterey Formation interface, the brittleness calculation drops to a value less than two. If the value of BRI is less than 2, empirical observation shows that the risk of embrittlement is lessened, and the confining layer is sufficiently ductile to accommodate large amounts of strain without undergoing brittle failure.

The average ductility of the confining zone based on the mean value from 18 wells is 1.24.

The average rock strength of the confining zone, as determined by the log derived UCS from the BRI calculations, is 2,452 psi.

As a result of the Reef Ridge Shale ductility, there are no fractures that will act as conduits for fluid migration from the Monterey Formation A1-A2 reservoir. This conclusion is supported by the following:

1. Extensive water and gas injection within the Monterey Formation confined by the Reef Ridge Shale within the AoR, the Greater Elk Hills Oil Field area and the San Joaquin Basin.
2. Prior to discovery, the Reef Ridge Shale provided seal to the underlying gas and oil reservoirs of the Monterey Formation for several million years.

Stress Field:

The stress of a rock can be expressed as three principal stresses. Formation fracturing will occur when the pore pressure exceeds the least of the stresses. in this circumstance, fractures will propagate in the direction perpendicular to the least principal stress (Figure 23).

Figure 23: Stress diagram showing the three principal stresses and the fracturing that will occur perpendicular to the minimum principal stress.

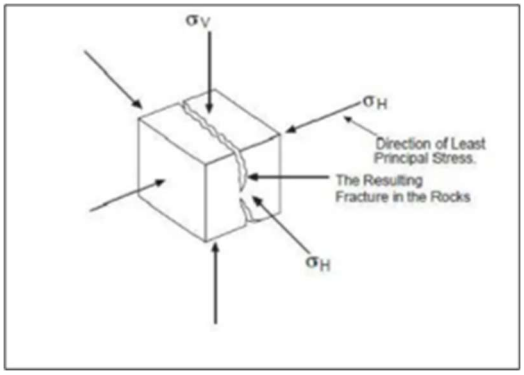

Elk Hills stresses have been studied in detail utilizing the large quantity of data recorded and available on fracture gradients and borehole breakout. Figure 24A shows that the maximum principal stress (SHmax) in the Elk Hills area is largely oriented northeast – southwest.

Figure 24A: Map showing the SHmax stress orientations in the Southern San Joaquin Basin (Castillo, 1997).

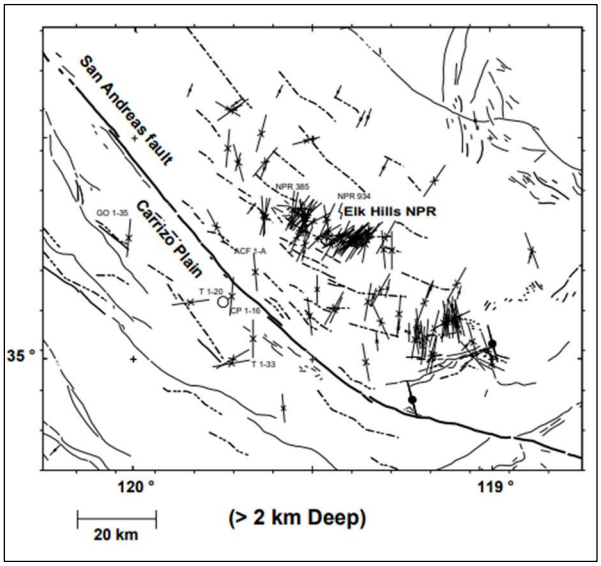

A1-A2 Fracture Gradient Test:

From a fracture test in well 362-18R-RD1, the Monterey Formation A1-A2 has a fracture gradient of 0.75 psi/ft, based on the initial shut-in pressure with an overburden gradient of 0.94 psi/ft and pore pressure gradient of 0.2 psi/ft. Using this gradient, the injectors are planned to be operated not to exceed 90% of the fracture pressure, which equates to a maximum allowable bottomhole gradient of 0.9*0.75 psi/ft = 0.675 psi/ft. Applying this gradient to the two injector locations, the maximum bottom injection pressures are shown in Table 3A.

Table 3A: Injectors 355-7R and 357-7R maximum allowable bottom hole injection pressure (psi) for the Monterey Formation A1-A2 injection zone.

Stress	357-7R	355-7R
Reservoir Fracture Gradient with Safety Factor (psi/ft)	0.675	0.675
Monterey Formation A1-A2 Injection Zone Perforation Top (ft TVD)	8,511	8,483
Fracture Pressure (psi)	5,745	5,726

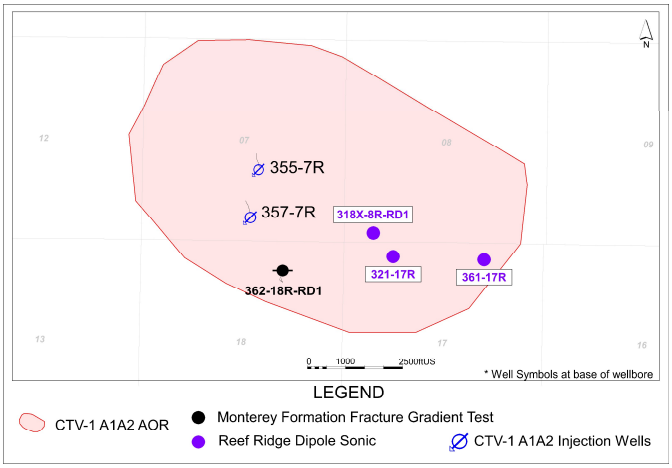

The method for calculating the overburden gradient was to integrate density logs using methodology laid out in Fjaer et al. (2008):

$$\sigma_v = \int_0^D \rho(z) g \, dz$$

where ρ is the density of the sediments, g is the acceleration due to gravity, D is the depth of interest, z is the vertical depth interval, and σ_v is the vertical stress (or overburden gradient). This calculation was completed using the "Overburden Gradient Calculation" module in the software Interactive Petrophysics 5.1.0. Figure 24B shows the calculation inputs and outputs for the 354X-7R well, which is within the AoR (see Figure 22 for well location).

Figure 24B: Example calculation of overburden gradient for the 354X-7R. Track 1: Correlation logs and caliper log. Track 2: Measured depth. Track 3: Vertical depth and vertical subsea depth. Track 4: Zones. Track 5: Resistivity. Track 6: Density and neutron porosity. Track 7: Overburden pressure (red) and overburden gradient (green).

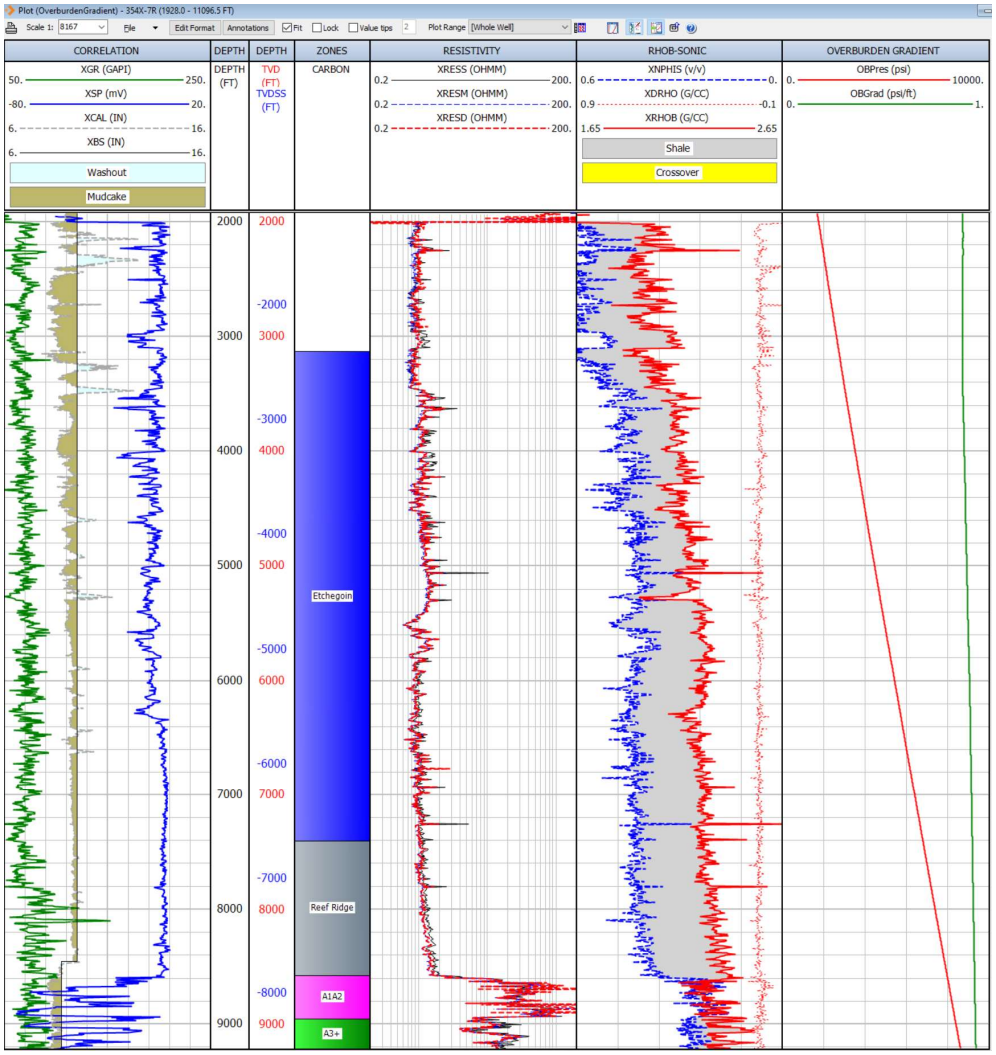

Reef Ridge Fracture Gradient:

The fracture gradient of the confining zone is determined by log-based calculation. California is an active tectonic regime, thereby CTV is using the Zhang (2017) method:

$$P_{FPavg} = \frac{3\nu}{2(1-\nu)}\left(S_v - P_p\right) + P_p$$

where S_h is the minimum horizontal stress, ν is Poisson's ratio, S_v is the overburden (vertical) stress, and P_p is the pore pressure.

Poisson's ratio is derived from dipole sonic logs (see the Geomechanical Modeling section – Geomechanical Modeling Parameters subsection of this document the calculation method). The average Poisson's Ratio of the Reef Ridge is 0.29. This is based on three wells containing 2,934 data points (see Table 3A for well locations). The overburden stress gradient was determined by integrating density logs. The Reef Ridge had an overburden gradient of 0.93 psi/ft based on 15 wells used to determine the average, comprising 52,331 data points. Being a shale, the pore pressure was assumed to be normally pressured.

Using these values, the calculated fracture gradient of the Reef Ridge confining zone is 0.74 psi/ft based on the Zhang, 2017 equation (Table 3B).

Table 3B: Calculated fracture gradient for the Confining Layer and the A2 shale.

Zone	Mean Poisson's Ratio (v/v)	Overburden Stress Gradient (psi/ft)	Pore Pressure Gradient (psi/ft)	Zhang's Fracture Gradient (psi/ft)
Confining Layer (Reef Ridge)	0.29	0.93	0.433	0.74
A2 shale	0.26	0.94	0.433	0.70

A2 Shale Fracture Gradient:

The average Poisson's Ratio of the A2 Shale is 0.26 based on three dipole sonic wells containing 133 data points (see Table 3A for dipole sonic log well locations). The overburden stress gradient was determined by integrating density logs. The A2 Shale had an overburden gradient of 0.94 psi/ft based on 15 wells used to determine the average, comprising 1,267 data points. Being a shale, the pore pressure was assumed to be normally pressured.

Using these values, the calculated fracture gradient of the A2 Shale is 0.7 psi/ft based on the Zhang, 2017 equation (Table 3B).

Geomechanical Modeling

Overview:

A finite element geomechanics module, GEOMECH, coupled with Computer Modeling Group's (CMG) equation of state compositional reservoir simulator (GEM), was used to model failure of the Reef Ridge Shale due to increasing pressure in the underlying reservoir by CO_2 injection. A modified Barton-Bandis model can be used to allow CO_2 to escape from the storage reservoir through the cap rock to overburden layers. The location and direction of fractures in a grid block are determined via normal fracture effective stress computed from the geomechanics module.

A generic two-dimensional model was constructed to represent the reservoir, confining layer, and overburden formations. CO_2 is injected through an injector located at the center of the X-Z plane and perforated throughout the reservoir. Increasing pressure in the reservoir is expected to push up and bend the overlying cap rock to create a tensile stress around the high-pressure region. As gas continues to be injected, the normal effective stress in the cap rock is expected to continually decrease. When the cap rock reaches a threshold value, defined as zero in this model, a crack will appear in the cap rock and the Barton-Bandis model will allow CO_2 to leak from the storage reservoir.

Results:

Failure pressures for the four scenarios are given in Table 4. The value for the reduced injection case was extrapolated from the pressure at a stress of about 10 psi These results suggest that the Reef Ridge Shale can tolerate a pressure at the base of 7,500 psi or more without failure.

Table 4: Geomechanical modeling results for four scenarios.

GEOMECHANICAL SCENARIO RESULTS	
SCENARIO	**FAILURE PRESSURE, psi**
BASE CASE	8,306
REDUCED YOUNG'S MODULUS	8,388
REDUCED INJECTION RATE	8,340
THINNER CAP ROCK	7,600

Description:

A 2-D cross-section model with 411 grid blocks in the X-direction and 33 grid blocks in the Z-direction was built encompassing a length of 43,100 feet and a thickness of 2,460 feet. This model is shown in Figure 25.

In the base model, the cap rock is 1,935 feet thick with a Young's modulus of 9E05 psi and a Poisson's ratio of 0.23. The reservoir is 525 feet thick with a Young's modulus of 7.25E05 psi and a Poisson's ratio of 0.25. Horizontal permeability is 1e-07 md in the cap rock and 40.5 md in the reservoir. The vertical to horizontal permeability ratio is 0.25. A constant porosity of 0.25 is used in all zones.

The reservoir is constrained at the bottom but allowed to move at the top and sides. The horizontal direction unconstrained boundary is used to cope with open regions on both the left and right of the modeled portion of the reservoir.

The injector was constrained to inject 30 million cubic feet per day of CO_2 with a maximum injection pressure of 10,000 psi.

Figure 25: Geomechanics Model.

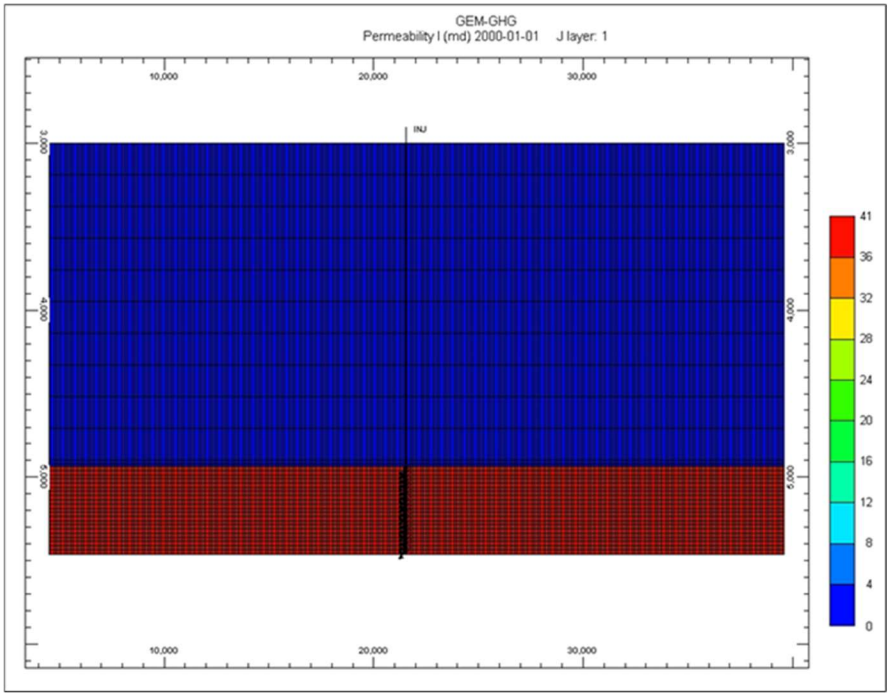

Scenarios Modeled:

Four scenarios were modeled in this study. In the base case, the cap rock has a Young's modulus of 9E05 psi. To model uncertainty in the cap rock Young's modulus, a second case was run with a value of 8E05 psi. In the third case, the impact of a thinner cap rock was modeled by assigning a confining layer of 795 feet. In the fourth case, sensitivity to injection rate was studied by reducing the injection rate to 20 million cubic feet per day.

Figure 26 gives the change in the normal fracture effective stress in the bottom cap rock layer and the pressure in the top layer of the reservoir with time for each scenario. The failure pressure is defined as the value at which the effective stress is zero. In the reduced injection rate case, the stress stopped decreasing at about 10 psi, due to CO_2 bleeding into the cap rock despite the very low vertical permeability.

Figure 26: Normal Fracture Stress and Pressure for Geomechanics Cases. Base case follows the reduced Young's Modulus case.

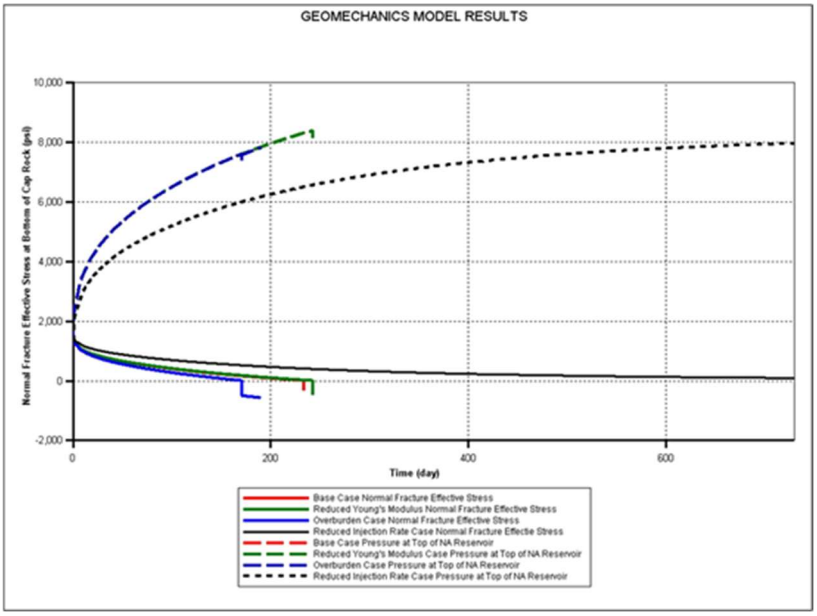

Geomechanical Modeling Parameters:

The geomechanical parameters used in the modeling were selected to represent a range of values for thickness, poisons ratio and Youngs Modulus. The following is a short description for parameter variability selection:

> **Thickness:** Reef Ridge thickness scenarios for the geomechanical modeling was 795 feet and 1,935 feet. The mean thickness of the Reef Ridge Shale confining layer overlying the

Monterey Formation A1-A2 AoR is 1,555 feet thick (Figure 12) as derived from open-hole log interpretation, which is between the parameters modeled.

Poisson's Ratio: Compressional and shear sonic logs were used to calculate Poisson's Ratio (Yale, 2017).

$$\nu_{dyn} = \nu_{stat} = \frac{V_p^2 - 2V_s^2}{2\left(V_p^2 - V_s^2\right)}$$

The following table shows the range of values determined for Poisons Ratio and that the parameters modeled are within the range or more conservative.

	Modeled			Actual		
	Base Case	2nd Case	3rd Case (1140' of Caprock)	P10	P50	P90
Caprock Reef Ridge	0.23	0.23	0.23	0.24	0.28	0.32
Reservoir A1-A2	0.25			0.19	0.25	0.3

Young's Modulus: Young's Modulus was calculated using compressional and shear sonic and bulk density logs. The dynamic to static correction applied was the Lacy shale method (Lacy, 1997):

$$E_{dyn} = \frac{\rho V_s^2\left(3V_p^2 - 4V_s^2\right)}{\left(V_p^2 - V_s^2\right)}$$

- See equation 8.1 in Fjaer et. al, 2008

$$E_{stat} = 0.0428E_{dyn}^2 + 0.2334E_{dyn}$$

- See equation 2 in Lacy, 1997.

The following table shows the range of values determined for Young's Modulus and that the parameters modeled are within the range or more conservative.

	Modeled			Actual		
	Base Case	2nd Case	3rd Case (Top 1140' of Caprock)	P10 E	P50 E	P90 E
Caprock Reef Ridge	0.9	0.8	0.6	0.66	0.91	1.36
Reservoir A1-A2	0.725			0.79	0.85	0.92

Seismic History [40 CFR 146.82(a)(3)(v)]

Seismic History:

The EHOF is in a seismically active region, but no active faults have been identified by the State Geologist of the California Division of Mines and Geology (CDMG) for the Elk Hills area (DOE, 1997). Active seismicity near the project site is related to the San Andreas Fault (located 12 miles west) and the White Wolf Fault (25 miles southeast from the EHOF). Activity on these faults occurs far deeper than the Monterey formation (~8,500 feet.) at about 6 miles below surface.

Historical seismic events were gathered from the publicly available Southern California Earthquake Data Center (SCEDC) and the USGS databases. Seismicity is monitored. The SCEDA is the most complete data set and has compiled all available historic seismic data holdings in southern California to create a single source for online access to southern California earthquake data. The Catalog goes back to the beginning of routine seismological operations by the Caltech Seismological Laboratory in 1932 (SCEDC website).

There have been no earthquakes in the AoR (Figure 27). In addition, there have only been eight earthquakes with a magnitude of 5.0 or greater within a 30-mile radius around the EHOF. The average depth of these earthquakes is 6.3 miles. Through monitoring via surface and borehole seismometer installation, CTV will establish a baseline and assess natural versus induced seismicity.

Figure 27: Earthquakes in the southern San Joaquin Basin with a magnitude greater than 3 since 1932. The White Wolf Fault is active in the southern San Joaquin Basin.

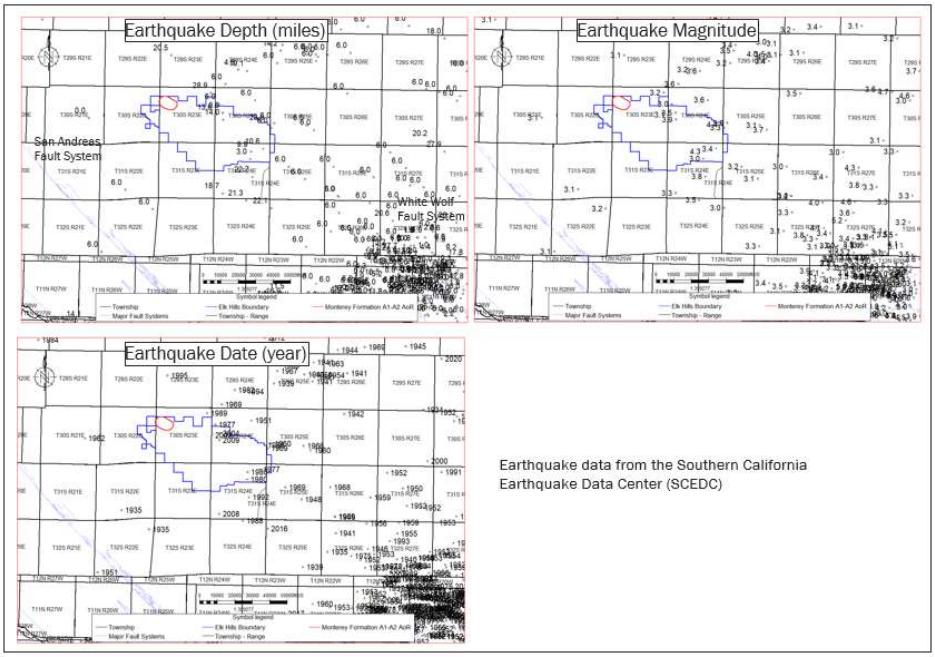

Seismic Risk:

The EHOF has been closely monitored for the effects of seismicity by CRC and previous owners and operators of the field. The San Joaquin Valley is seismically active outside the EHOF, but no basin wide events have impacted the Elk Hills reservoirs and oil and gas infrastructure. This is due, in part, to the thickness and high level of clay in the primary confining layer Reef Ridge Shale.

The following is a summary of CTVs seismic risk:

Has a geologic system free of known active faults and fractures and capable of receiving and containing the volumes of CO2 proposed to be injected.

- Extensive historical operations in the Monterey Formation A1-A2 reservoir is valuable experience to understand operating conditions such as injection volumes and reservoir containment. The strategy to limit the injected CO2 to at or beneath the initial reservoir pressure will mitigate the potential for induced seismic events and endangerment of the USDW.
- No active faults have been identified by the State Geologist of the California Division of Mines and Geology (CDMG) for the Elk Hills area.
- VS30, defined as the average seismic shear-wave velocity (VS) from the surface to a depth of 30 meters. Mapping completed by the USGS shows that the EHOF has very dense soil and soft rock based on the National Earthquake Hazards Reduction Program site classification. The high Vs30 (Figure 28) means that the site has thin sediment and low factor amplification, reducing risk to surface facilities, wells, and other infrastructure.
- There are no faults or fractures identified in the AoR that will impact the confinement of CO_2 injectate.

Will be operated and monitored in a manner that will limit risk of endangerment to USDWs, including risks associated with induced seismic events;

- The strategy to limit the injected CO_2 to at or beneath the initial reservoir pressure will mitigate the potential for induced seismic events and endangerment of the USDW.
- Injection pressure will be lower than the fracture gradients of the sequestration reservoir (90% of the fracture gradient) and confining layer.
- Injection and monitoring well pressure monitoring will ensure that pressures are beneath the fracture pressure of the sequestration reservoir and confining zone. Injection pressure will be lower than the fracture gradients of the sequestration reservoir (90% of the fracture gradient) and confining layer.
- A seismic monitoring program will be designed to detect events lower than seismic events that can be felt. This will ensure that operations can be modified with early warning events, before a felt seismic event.

Figure 28: VS30 analysis from the USGS that supports the EHOF has a low risk for shallow well and infrastructure impact due to earthquakes.

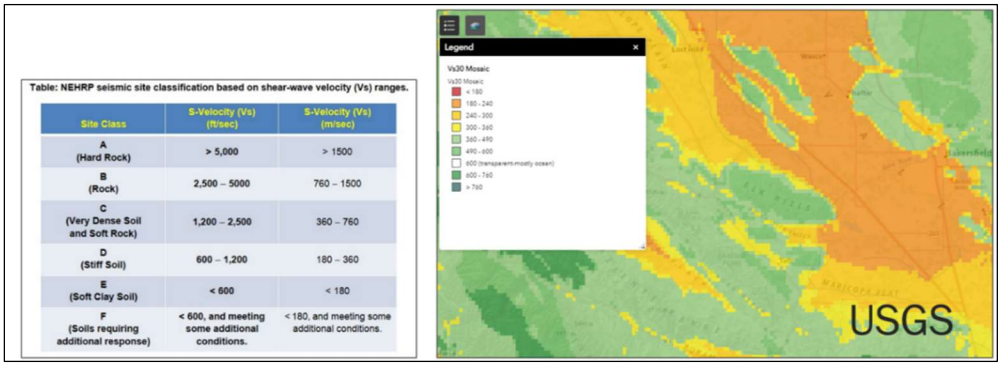

Table: NEHRP seismic site classification based on shear-wave velocity (Vs) ranges.

Site Class	S-Velocity (Vs) (ft/sec)	S-Velocity (Vs) (m/sec)
A (Hard Rock)	> 5,000	> 1500
B (Rock)	2,500 – 5000	760 – 1500
C (Very Dense Soil and Soft Rock)	1,200 – 2,500	360 – 760
D (Stiff Soil)	600 – 1,200	180 – 360
E (Soft Clay Soil)	< 600	< 180
F (Soils requiring additional response)	< 600, and meeting some additional conditions.	< 180, and meeting some additional conditions.

Will be operated and monitored in a way that in the unlikely event of an induced event, risks will be quickly addressed and mitigated; and

- Via monitoring and surveillance practices (pressure and seismic monitoring program) CTV personnel will be notified of events that are considered an early warning sign. Early warning signs will be addressed to ensure that more significant events do not occur.
- CTV will establish a central control center to ensure that personnel have access to the continuous data being acquired during operations.

Poses a low risk of inducing a felt seismic event.

- Pressure will be monitored in each injector and sequestration monitoring well to ensure that pressure does not exceed the fracture pressure of the reservoir or confining layer.
- A seismic monitoring program will be designed to detect events lower than seismic events that can be felt. This will ensure that operations can be modified with early warning events, before a felt seismic event.
- The operational strategy of keeping the reservoir pressure at or beneath the initial pressure of the reservoir has been designed to reduce the risk for seismic events.

Hydrologic and Hydrogeologic Information [40 CFR 146.82(a)(3)(vi), 146.82(a)(5)]

In the Elk Hills area, the Tulare Formation conformably overlies the shallow marine deposits of the San Joaquin Formation (Figure 29). CTV has studied the shallow aquifers at the EHOF extensively. Within the regional and site-specific area, the Tulare Formation is the only aquifer that contains water less than 10,000 mg/l TDS. There are no water wells nor springs within the AoR.

Figure 29: Cross-section showing the Tulare Formation USDW. The Lower Tulare is an exempt aquifer (2018). The Upper Tulare air sands have 3,000 – 10,000 TDS water at the base, on the edges of the Northwest Stevens anticline.

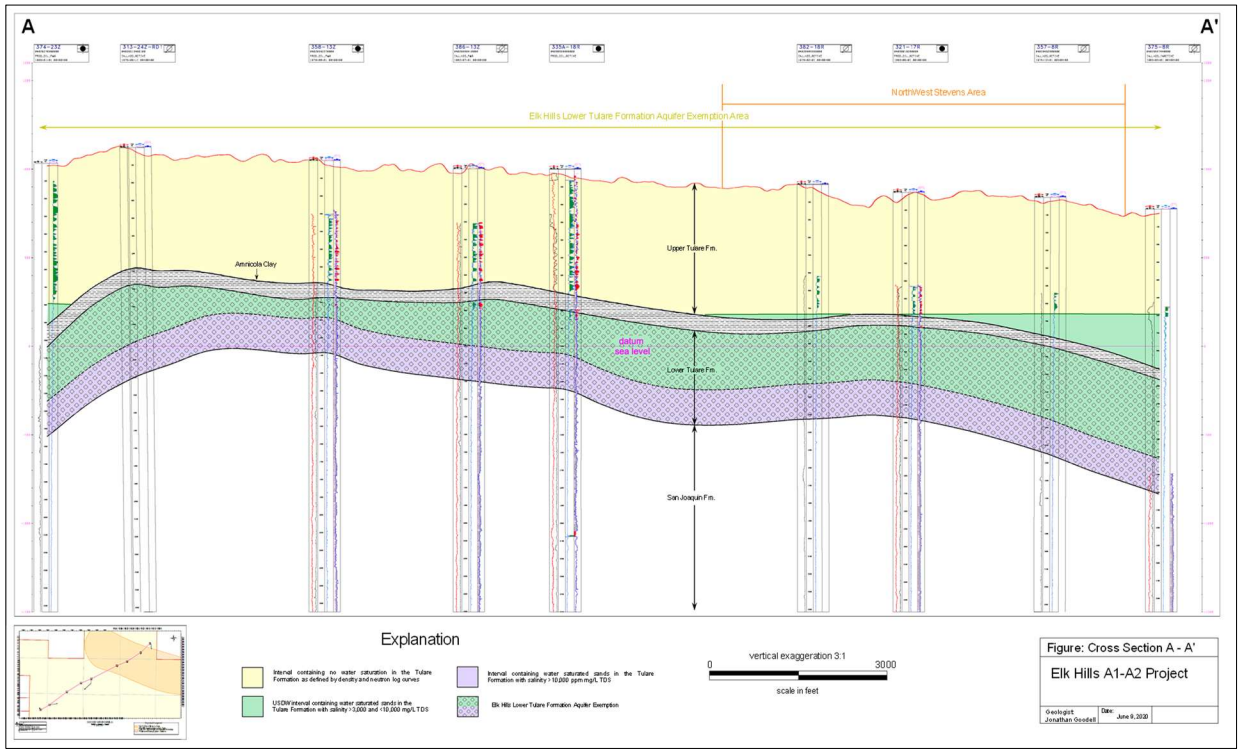

The Tulare Formation is Pliocene aged and is comprised of a thick succession of nonmarine sandstone, conglomerate, and shale beds. It is subdivided into the Upper and Lower Tulare separated by the sealing Amnicola Claystone (Figure 29). The depth is 600 - 2,500 feet and the thickness ranges from 1,200 - 1,750 feet (Figure 30).

Figure 30: Tulare Formation isopach map.

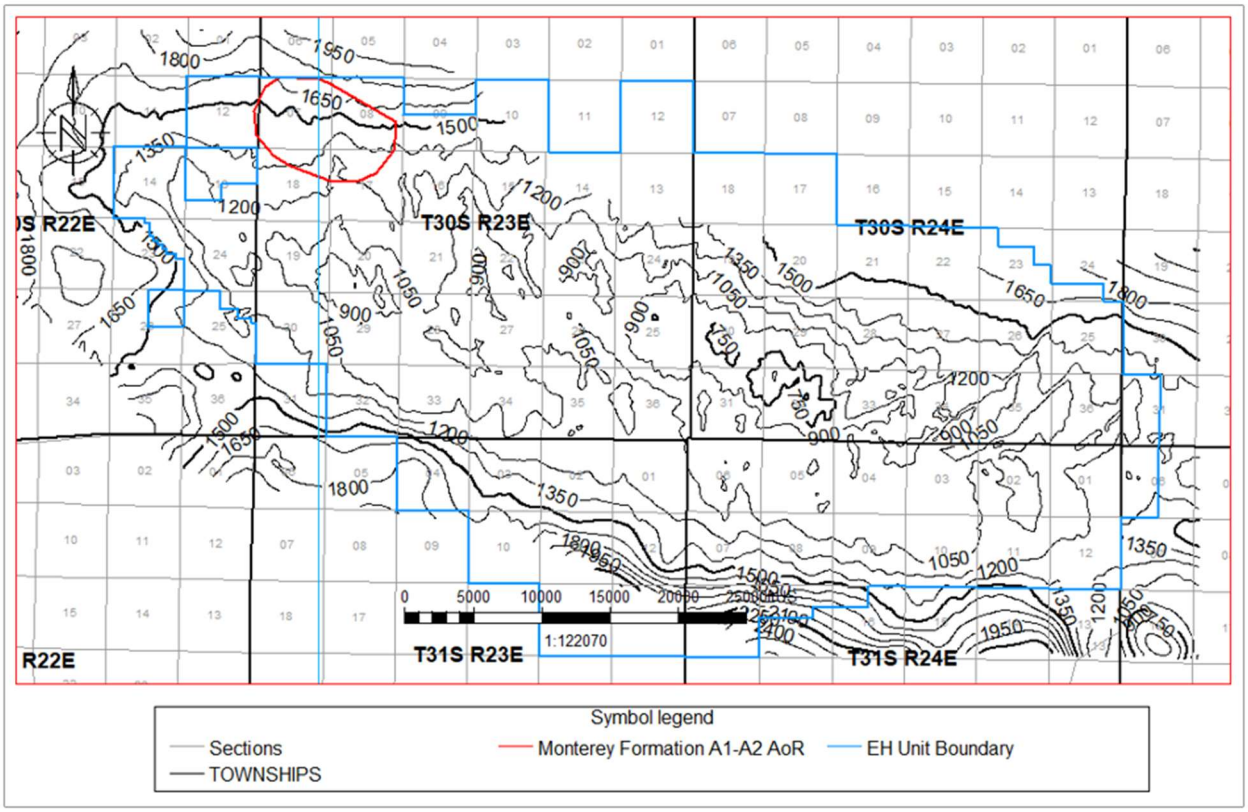

The upper intervals of the Tulare Formation consist of sand beds that that are completely dry or at irreducible water saturated and are referred to as the unsaturated zone. In the AoR the unsaturated zone is within the Upper Tulare USDW. The air sands-water contact in the Upper Tulare is determined from resistivity, density, and neutron geophysical logs (Figure 31). The characteristic density-neutron crossover (orange-filled intervals) is caused by the lack of fluid in the porous formation sands, and results in very low measured bulk density and very low measured neutron porosity.

Figure 31 shows the Upper Tulare USDW overlain by the Upper Tulare air sands. The Upper Tulare is 850 feet in depth and is separated from the underlying Reef Ridge Shale confining layer by 6,450 feet and the Monterey Formation A1-A2 sequestration reservoir by 7,650 feet.

Figure 31: Type log for the Tulare Formation showing the Upper Tulare unsaturated zone, Upper Tulare USDW and Lower Tulare exempt aquifer.

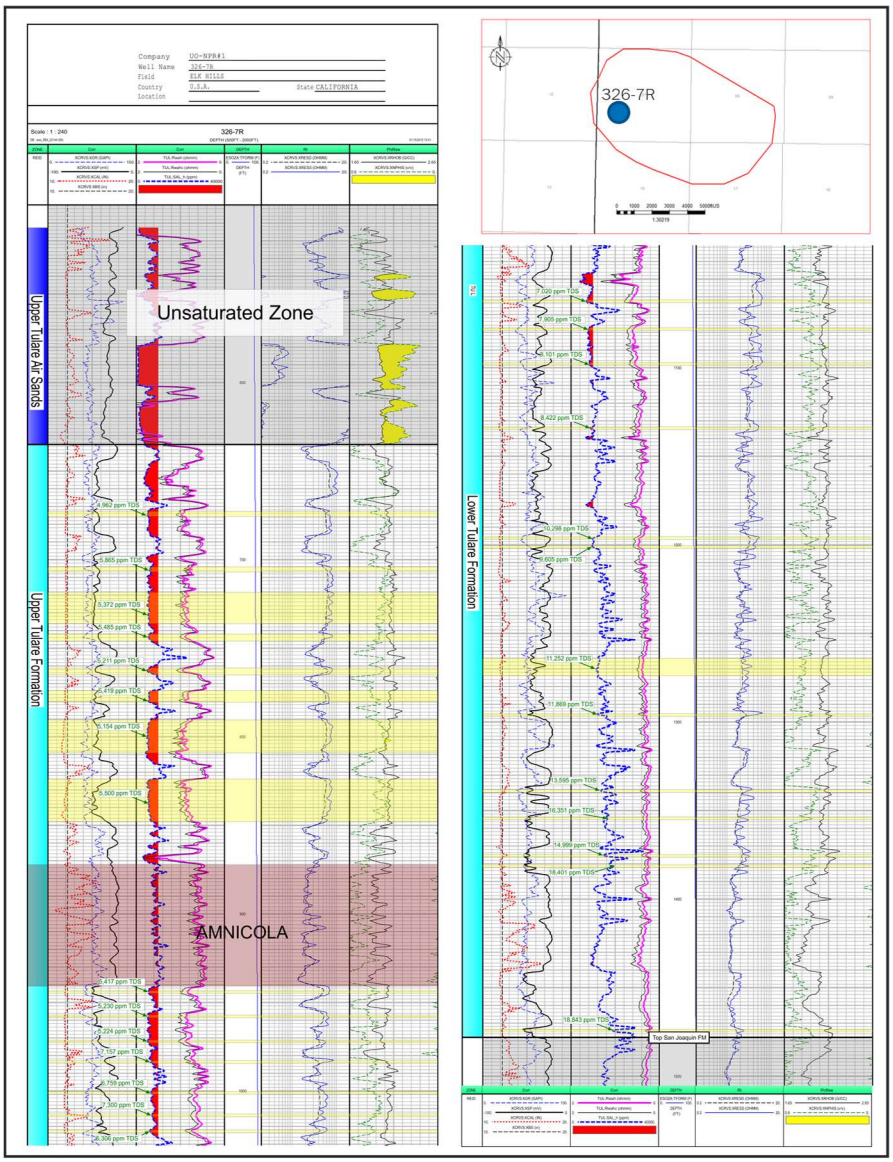

Salinity Calculation

Calculation of salinity as shown in Figure 31 is a four-step process:

(1) converting measured density to formation porosity

The equation to convert measured density to porosity is:

POR = (Rhom - RHOB) /(Rhom-Rhof)

Parameter definitions for the equation are:

POR is formation porosity

Rhom is formation matrix density grams per cubic centimeters (g/cc); 2.65 g/cc is used for sandstones

RHOB is calibrated bulk density taken from well log measurements (g/cc)
Rhof is fluid density (g/cc); 1.00 g/cc is used for water-filled porosity

(2) calculation of apparent water resistivity using the Humble equation,

The Humble equation calculates apparent water resistivity. The equation is:

Rwah = ((POR**m) * XRESD)/a

Parameter definitions for the equation are:

Rwah is apparent water resistivity (ohmm)
POR is formation porosity as derived from the density conversion formula
m is the cementation factor; 2.15 is the standard value
XRESD is deep reading resistivity taken from well log measurements (ohmm)
a is the archie constant; 0.62 is the standard value

(3) correcting apparent water resistivity to a standard temperature

Apparent water resistivity is corrected from formation temperature to a surface temperature standard of 75 degrees Fahrenheit:

Rwahc = Rwah * ((TEMP)+6.77)/(75+6.77)

Parameter definitions for the equation are:

Rwahc is apparent water resistivity (ohmm), corrected to surface temperature
TEMP is down hole temperature based on temperature gradient (DegF)

(4) converting temperature corrected apparent water resistivity to salinity.

The following formular was used:

SAL_h = 10 ** ((3.562-(Log10(Rwahc-0.0123)))/.955)

Parameter definitions for the equation are:

SAL_h is salinity from corrected Rwahc (ppm)
Rwahc is apparent water resistivity, corrected to surface temperature (ohmm),

Water Samples

Tulare Formation water within the AoR and the Elk Hill Oil Field is not utilized due to high TDS (3,000 – 10,000 mg/l) and concentrations of heavy metals above maximum containment levels (MCL).

Figure 32: Lower Tulare aquifer exemption boundary.

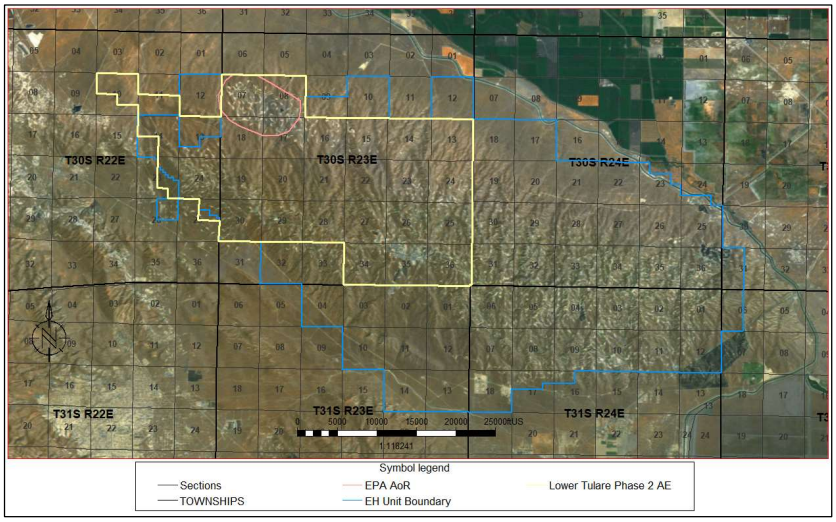

In 2018 the Lower Tulare aquifer (boundary shown on map in Figure 32) was exempted because the water meets the federal exemption criteria:

1. The portion of the formation for exemption in the field does not serve as a source of drinking water; and
2. The portion of the formation proposed for exemption in the field has more than 3,000 milligrams per liter (mg/L) and less than 10,000 mg/l TDS content and is not reasonably expected to supply a public water system.

The Upper Tulare USDW has 3,000-10,000 mg/l TDS on the edges of the NWS anticline. Water quality for the Upper Tulare USDW is shown in Figure 33. The water is not used within the AoR or the EHOF.

Figure 33: Upper Tulare USDW and Lower Tulare Formation water analysis.

Upper Tulare

Table 6a. WATER SOURCE WELL #43WS-13B
WATER ANALYSIS DATA (mg/kg)

DATE	6-95	7-95	8-95	9-95
SAMPLE #	95094	95150	95182	95189
CONSTITUENTS:				
Calcium, Ca	230	230	220	220
Magnesium, Mg	85	85	92	93
Sodium, Na	1280	1300	1200	1300
Potassium, K	9.2	9.8	8.8	8.6
Iron, Fe	0.4	0.51	0.38	0.54
Hydroxide, OH	0	0	0	0
Carbonate, CO3	0	0	0	0
Bicarb, HCO3	180	190	190	180
Chloride, Cl	1360	1400	1300	1400
Sulfate, SO4	1600	1600	1500	1600
Sulfide, S	<5.0	<5.0	<5.0	<5.0
Totals	4660	4700	4400	4700
Boron, B	4.7	4.6	4.7	4.7
TDS (Grav)	4890	4800	4900	4900
Hardness, CaCO3	920	920	930	930
Alkalinity, CaCO3	150	160	160	150
Sodium Chloride	3690	3700	3500	3800
pH	7.8	8.1	8.0	7.9
Electrical Conductivity	6.99 mmhos/cm	7.02 mmhos/cm	6.99 mmhos/cm	6.99 mmhos/cm
Specific Gravity	1.003	1.003	1.004	1.003
Resistivity	1.43 ohmm	1.43 ohmm	1.43 ohmm	1.43 ohmm

NOTE: Sample analysis is from Zalco Laboratory.

(Source: NPR-1 Ground Water Monitoring Plan, 1995)

Lower Tulare

Water Analysis (General Chemistry)

BCL Sample ID: 1411084-01 | Client Sample Name: Elk Hills Well 82-2B, 5/17/2014 4:05:00PM, Rick Ogletree

Constituent	Result	Units	PQL	MDL	Method	MB Bias	Lab Quals
Electrical Conductivity @ 25 C (Field Test)	27000	umhos/cm	1.0	1.0	EPA-120.1		
pH (Field Test)	7.23	pH Units	0.05	0.05	EPA-150.1		
Temperature (Field Test)	87.6	F	32.0	32.0	SM-2550B		
Total Calcium	650	mg/L	2.0	0.30	EPA-6010B	ND	A10
Total Magnesium	230	mg/L	1.0	0.38	EPA-6010B	0.75	A10
Total Sodium	4700	mg/L	10	1.0	EPA-6010B	ND	A01
Total Potassium	31	mg/L	20	2.6	EPA-6010B	ND	A10
Bicarbonate Alkalinity as CaCO3	59	mg/L	8.2	8.2	EPA-310.1	ND	
Carbonate Alkalinity as CaCO3	ND	mg/L	8.2	8.2	EPA-310.1	ND	
Hydroxide Alkalinity as CaCO3	ND	mg/L	8.2	8.2	EPA-310.1	ND	
Total Alkalinity as CaCO3	59	mg/L	8.2	8.2	EPA-310.1	ND	
Bromide	50	mg/L	5.0	2.2	EPA-300.0	ND	A01
Chloride	10000	mg/L	50	6.7	EPA-300.0	20	A01
Fluoride	ND	mg/L	2.5	0.70	EPA-300.0	ND	A10
Nitrate as NO3	ND	mg/L	22	5.5	EPA-300.0	ND	A10
Sulfate	320	mg/L	50	9.0	EPA-300.0	19	A01
pH	7.47	pH Units	0.05	0.05	EPA-150.1		S05
Electrical Conductivity @ 25 C	26100	umhos/cm	1.00	1.00	EPA-120.1		
Total Dissolved Solids @ 180 C	20000	mg/L	1000	1000	EPA-160.1	ND	

Ground Water Flow

The Elk Hills field is located within an area of the San Joaquin Basin which has only interior drainage and no appreciable surface or subsurface outflow. The Kern River, which is the primary source of surface water and fresh groundwater in the area, drains to the southeast and terminates near the northeastern side of the Elk Hills field. Precipitation in the Elk Hills area averages about 5.8 inches annually, with an average pan evaporation rate of about 108 inches per year in the Buttonwillow area. As a result, almost no groundwater from precipitation recharges the Tulare Formation groundwater, causing salts to become more concentrated over time and potentially resulting in high TDS concentrations.

Water Supply Wells

All available water supply well databases were reviewed for information on water wells in the site-specific area and proximity. This includes CalGEM, USGS, the Kern County Water Agency (KCWA), West Kern Water District, the California Department of Water Resources, and the GeoTracker Groundwater Ambient Monitoring and Assessment (GAMA) online database. CTV owns the surface area of the Elk Hills Unit in its entirety, and there are no records of water supply wells within the AoR.

Geochemistry [40 CFR 146.82(a)(6)]

Geochemistry A1-A2 Reservoir:

The Monterey Formation A1-A2 reservoir has a gas cap that overlies a thin oil band and a basal water zone. CRC and previous operators have collected baseline data used to characterize the reservoir. Produced fluid sampled during oil and gas operations is used to characterize the Monterey Formation A1-A2 geo-chemistry, this includes water and hydrocarbons (gas and oil). Geochemical results for the hydrocarbon and water analysis and total dissolved solids have been used as inputs for computational modeling.

Figure 34 shows the water chemistry from well 381-17R, taken from a sand underlying the Monterey Formation A1-A2 reservoir. Reservoir depletion of the Monterey Formation A1-A2 has reduced the water saturation to residual, preventing representative water sampling.

Figure 34: Monterey Formation A1-A2 reservoir water geochemistry from well 381-17R. Monterey Formation total dissolved solids based on well 381-17R is 24,877, well above USDW standards.

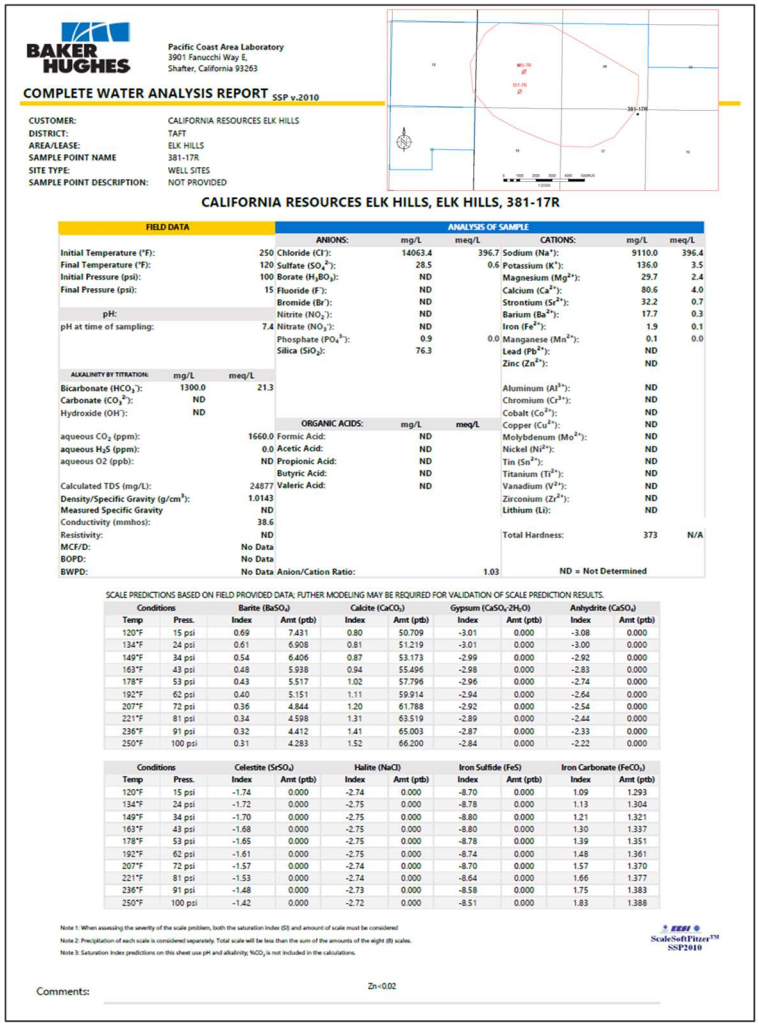

BAKER HUGHES

Pacific Coast Area Laboratory
3901 Fanucchi Way E,
Shafter, California 93263

COMPLETE WATER ANALYSIS REPORT SSP v.2010

CUSTOMER:	CALIFORNIA RESOURCES ELK HILLS
DISTRICT:	TAFT
AREA/LEASE:	ELK HILLS
SAMPLE POINT NAME	381-17R
SITE TYPE:	WELL SITES
SAMPLE POINT DESCRIPTION:	NOT PROVIDED

CALIFORNIA RESOURCES ELK HILLS, ELK HILLS, 381-17R

FIELD DATA	
Initial Temperature (°F):	250
Final Temperature (°F):	120
Initial Pressure (psi):	100
Final Pressure (psi):	15
pH:	
pH at time of sampling:	7.4

ALKALINITY BY TITRATION:	mg/L	meq/L
Bicarbonate (HCO_3^-):	1300.0	21.3
Carbonate (CO_3^{2-}):	ND	
Hydroxide (OH^-):	ND	
aqueous CO_2 (ppm):	1660.0	
aqueous H_2S (ppm):	0.0	
aqueous O2 (ppb):	ND	
Calculated TDS (mg/L):	24877	
Density/Specific Gravity (g/cm³):	1.0143	
Measured Specific Gravity	ND	
Conductivity (mmhos):	38.6	
Resistivity:	ND	
MCF/D:	No Data	
BOPD:	No Data	
BWPD:	No Data	

ANALYSIS OF SAMPLE — ANIONS:	mg/L	meq/L
Chloride (Cl^-):	14063.4	396.7
Sulfate (SO_4^{2-}):	28.5	0.6
Borate (H_3BO_3):	ND	
Fluoride (F^-):	ND	
Bromide (Br^-):	ND	
Nitrite (NO_2^-):	ND	
Nitrate (NO_3^-):	ND	
Phosphate (PO_4^{3-}):	0.9	0.0
Silica (SiO_2):	76.3	

ORGANIC ACIDS:	mg/L	meq/L
Formic Acid:	ND	
Acetic Acid:	ND	
Propionic Acid:	ND	
Butyric Acid:	ND	
Valeric Acid:	ND	

CATIONS:	mg/L	meq/L
Sodium (Na^+):	9110.0	396.4
Potassium (K^+):	136.0	3.5
Magnesium (Mg^{2+}):	29.7	2.4
Calcium (Ca^{2+}):	80.6	4.0
Strontium (Sr^{2+}):	32.2	0.7
Barium (Ba^{2+}):	17.7	0.3
Iron (Fe^{2+}):	1.9	0.1
Manganese (Mn^{2+}):	0.1	0.0
Lead (Pb^{2+}):	ND	
Zinc (Zn^{2+}):	ND	
Aluminum (Al^{3+}):	ND	
Chromium (Cr^{2+}):	ND	
Cobalt (Co^{2+}):	ND	
Copper (Cu^{2+}):	ND	
Molybdenum (Mo^{2+}):	ND	
Nickel (Ni^{2+}):	ND	
Tin (Sn^{2+}):	ND	
Titanium (Ti^{2+}):	ND	
Vanadium (V^{2+}):	ND	
Zirconium (Zr^{2+}):	ND	
Lithium (Li^-):	ND	
Total Hardness:	373	N/A

Anion/Cation Ratio: 1.03 — ND = Not Determined

SCALE PREDICTIONS BASED ON FIELD PROVIDED DATA; FUTHER MODELING MAY BE REQUIRED FOR VALIDATION OF SCALE PREDICTION RESULTS.

Conditions		Barite ($BaSO_4$)		Calcite ($CaCO_3$)		Gypsum ($CaSO_4 \cdot 2H_2O$)		Anhydrite ($CaSO_4$)	
Temp	Press.	Index	Amt (ptb)	Index	Amt (ptb)	Index	Amt (ptb)	Index	Amt (ptb)
120°F	15 psi	0.69	7.431	0.80	50.709	-3.01	0.000	-3.08	0.000
134°F	24 psi	0.61	6.908	0.81	51.219	-3.01	0.000	-3.00	0.000
149°F	34 psi	0.54	6.406	0.87	53.173	-2.99	0.000	-2.92	0.000
163°F	43 psi	0.48	5.938	0.94	55.496	-2.98	0.000	-2.83	0.000
178°F	53 psi	0.43	5.517	1.02	57.796	-2.96	0.000	-2.74	0.000
192°F	62 psi	0.40	5.151	1.11	59.914	-2.94	0.000	-2.64	0.000
207°F	72 psi	0.36	4.844	1.20	61.788	-2.92	0.000	-2.54	0.000
221°F	81 psi	0.34	4.598	1.31	63.519	-2.89	0.000	-2.44	0.000
236°F	91 psi	0.32	4.412	1.41	65.003	-2.87	0.000	-2.33	0.000
250°F	100 psi	0.31	4.283	1.52	66.200	-2.84	0.000	-2.22	0.000

Conditions		Celestite ($SrSO_4$)		Halite (NaCl)		Iron Sulfide (FeS)		Iron Carbonate ($FeCO_3$)	
Temp	Press.	Index	Amt (ptb)	Index	Amt (ptb)	Index	Amt (ptb)	Index	Amt (ptb)
120°F	15 psi	-1.74	0.000	-2.74	0.000	-8.70	0.000	1.09	1.293
134°F	24 psi	-1.72	0.000	-2.75	0.000	-8.78	0.000	1.13	1.304
149°F	34 psi	-1.70	0.000	-2.75	0.000	-8.80	0.000	1.21	1.321
163°F	43 psi	-1.68	0.000	-2.75	0.000	-8.80	0.000	1.30	1.337
178°F	53 psi	-1.65	0.000	-2.75	0.000	-8.78	0.000	1.39	1.351
192°F	62 psi	-1.61	0.000	-2.75	0.000	-8.74	0.000	1.48	1.361
207°F	72 psi	-1.57	0.000	-2.74	0.000	-8.70	0.000	1.57	1.370
221°F	81 psi	-1.53	0.000	-2.74	0.000	-8.64	0.000	1.66	1.377
236°F	91 psi	-1.48	0.000	-2.73	0.000	-8.58	0.000	1.75	1.383
250°F	100 psi	-1.42	0.000	-2.72	0.000	-8.51	0.000	1.83	1.388

Note 1: When assessing the severity of the scale problem, both the saturation index (SI) and amount of scale must be considered
Note 2: Precipitation of each scale is considered separately. Total scale will be less than the sum of the amounts of the eight (8) scales.
Note 3: Saturation Index predictions on this sheet use pH and alkalinity; $%CO_2$ is not included in the calculations.

SSI ® ScaleSoftPitzer™ SSP2010

Comments: Zn<0.02

The hydrocarbon composition for the Monterey Formation A1-A2 reservoir was determined using chromatography in conjunction with low temperature, fractional distillation. Figure 35 shows the results of the hydrocarbon composition for well 335-7R within the AoR. Oil composition analysis was routinely completed upon reservoir discovery and was collected across the field. This original dataset is valid for the oil composition, as the hydrocarbon components are consistent to the present time.

Figure 35: Monterey Formation A1-A2 hydrocarbon geochemistry from well 335-7R in 1974.

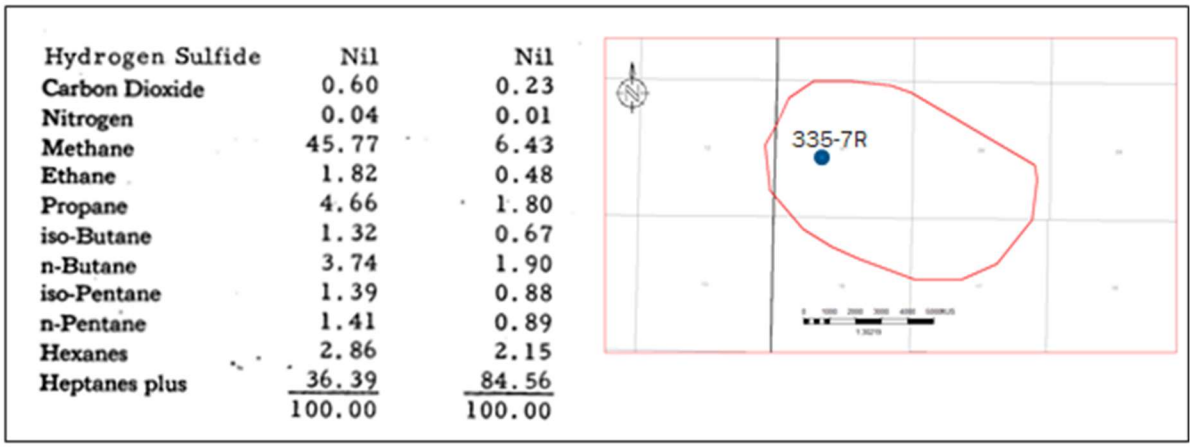

Hydrogen Sulfide	Nil	Nil
Carbon Dioxide	0.60	0.23
Nitrogen	0.04	0.01
Methane	45.77	6.43
Ethane	1.82	0.48
Propane	4.66	1.80
iso-Butane	1.32	0.67
n-Butane	3.74	1.90
iso-Pentane	1.39	0.88
n-Pentane	1.41	0.89
Hexanes	2.86	2.15
Heptanes plus	36.39	84.56
	100.00	100.00

Gas composition for the Monterey Formation A1-A2 is collected to assess the changing concentration of key components. Since 2011, CTV has used two injectors for reservoir pressure support; 357-7R and 355-7R to inject gas containing up to 44% CO_2. Figure 36 shows the produced natural gas analysis for 353-7R in 2021. Note that the composition has 6.5 mole % CO_2.

Figure 36: Natural gas composition analysis for well 353-7R in 2021.

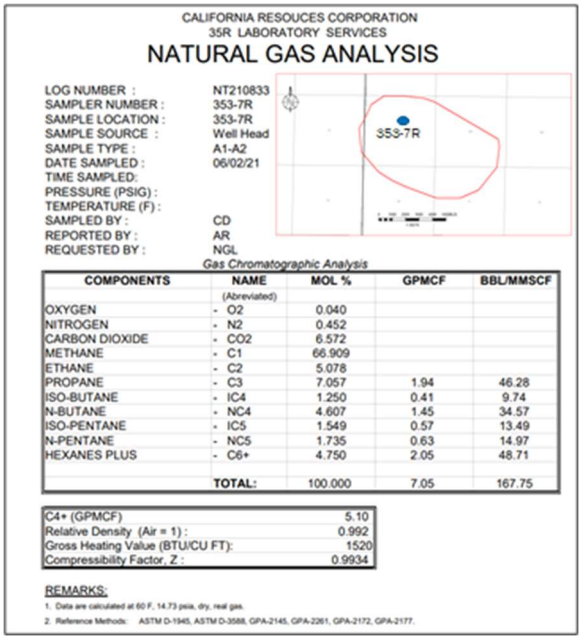

CALIFORNIA RESOUCES CORPORATION
35R LABORATORY SERVICES

NATURAL GAS ANALYSIS

LOG NUMBER :	NT210833
SAMPLER NUMBER :	353-7R
SAMPLE LOCATION :	353-7R
SAMPLE SOURCE :	Well Head
SAMPLE TYPE :	A1-A2
DATE SAMPLED :	06/02/21
TIME SAMPLED:	
PRESSURE (PSIG) :	
TEMPERATURE (F) :	
SAMPLED BY :	CD
REPORTED BY :	AR
REQUESTED BY :	NGL

Gas Chromatographic Analysis

COMPONENTS	NAME (Abreviated)	MOL %	GPMCF	BBL/MMSCF
OXYGEN	- O2	0.040		
NITROGEN	- N2	0.452		
CARBON DIOXIDE	- CO2	6.572		
METHANE	- C1	66.909		
ETHANE	- C2	5.078		
PROPANE	- C3	7.057	1.94	46.28
ISO-BUTANE	- IC4	1.250	0.41	9.74
N-BUTANE	- NC4	4.607	1.45	34.57
ISO-PENTANE	- IC5	1.549	0.57	13.49
N-PENTANE	- NC5	1.735	0.63	14.97
HEXANES PLUS	- C6+	4.750	2.05	48.71
	TOTAL:	100.000	7.05	167.75

C4+ (GPMCF)	5.10
Relative Density (Air = 1) :	0.992
Gross Heating Value (BTU/CU FT):	1520
Compressibility Factor, Z :	0.9934

REMARKS:

1. Data are calculated at 60 F, 14.73 psia, dry, real gas.
2. Reference Methods: ASTM D-1945, ASTM D-3588, GPA-2145, GPA-2261, GPA-2172, GPA-2177.

Monterey Formation A1-A2 Reactions:

Mineralogy and formation fluid interactions have been assessed for the Monterey Formation. The following applies to potential reactions associated with the CO_2 injectate:

1. The Monterey Formation A1-A2 reservoir has a low current water volume (~15% saturation in the gas cap and 85% in the thin oil leg) due to production related to oil and gas operations, where four million net barrels of water have been produced. This low volume of water will minimize both the quantity of CO_2 that will dissolve in solution and the quantity of carbonic acid formed in-situ.
2. Residual oil saturation (15%) in the Monterey Formation A1-A2 reservoir will also dissolve only a small amount of CO_2.
3. The Monterey Formation A1-A2 has a negligible quantity of carbonate minerals and is instead dominated by quartz and feldspar. These minerals are stable in the presence of CO_2 and carbonic acid and any dissolution or changes that occur will be on grain surfaces.
4. Since 2011 6.3 billion cubic feet of gas has been injected in the 357-7R and 355-7R wells, consisting of up to 44% CO_2. Injectivity of the reservoir has not changed.

The oil and water CO2 trapping mechanisms have been incorporated in the computational modeling and will be discussed in the AoR and Corrective Action Plan.

Reef Ridge Shale Confining Layer Reactions:

There is no geochemistry analysis for the Reef Ridge Shale. The shale will only provide fluid for analysis if stimulated. However, given the low permeability of the rock, high capillary entry pressure, and the low carbonate content, the Reef Ridge Shale is not expected to be impacted by the CO2 injectate.

Geochemical Modeling of A1-A2 Monterey Formation and Reef Ridge Shale:

Geochemical modeling has been carried out to understand the potential interactions of the injectate with the formation mineralogy and fluids. The modeling was carried out for the A1-A2 Monterey formation injection zone and for the Reef Ridge shale confining zone, using the USGS geochemical modeling software PHREEQC (ph-REdox-Equilibrium).

The model was set up using the formation fluid data referenced in the "Geochemistry A1-A2 Reservoir" section and using mineralogy data referenced in the "Mineralogy" section of this document. The injectate compositions used for the modeling are detailed in the "Appendix 3: A1-A2 Geochemical modeling" and in the "Proposed Carbon Dioxide Stream" section of the Attachment B document.

The Geochemical modeling indicates, as expected, that due to the dominant stable quartz and feldspar mineralogy of the formation, only minimal amounts of minerals will dissolve and precipitate. The net modeled change in molar mass was minimal with a decrease in mass, ranging from 1 percent to 0.2 percent in the Monterey Formation. The Reef Ridge had a 0.8 percent

increase. As such the Injection zone, Confining zone and Formation fluids can be considered compatible with the proposed injectates, with the geochemical modeling indicating no significant reactions that might affect injection and storage at the site.

Details of the modeling methodology and results can be found in "Appendix 3: A1-A2 Geochemical modeling".

CTV will review and confirm the geochemical modeling as part of pre-operational testing based on injectate sampling to ensure that they are consistent with the model inputs.

Site Suitability [40 CFR 146.83]

The Monterey Formation A1-A2 reservoir in the Northwest Stevens anticline was discovered in the 1970's. For over 40 years the reservoir has been developed with the injection of water and gas to maintain reservoir pressure for improved oil recovery, Class II injection approved by CalGEM. This operating experience provides an intimate knowledge of the confining Reef Ridge Shale and the hydrodynamics of the Monterey Formation A1-A2 reservoir.

In support of the EPA Class VI application, CTV has fully characterized the site for suitability by integrating static data that includes well logs, three dimensional seismic and core data, as well as dynamic data that includes reservoir production, injection, and pressure data. Figure 37 shows the continuity of the A1-A2 reservoir and illustrates representative logs data collected during drilling used to develop the static model. The operational strategy of maintaining final reservoir pressure at or below the discovery pressure of the reservoir mitigates future confinement concerns.

Figure 37: Cross section showing continuity of the A1-A2 reservoir and underlying A2 Shale. Logs shown are representative of those collected during drilled and used to develop the static geological model.

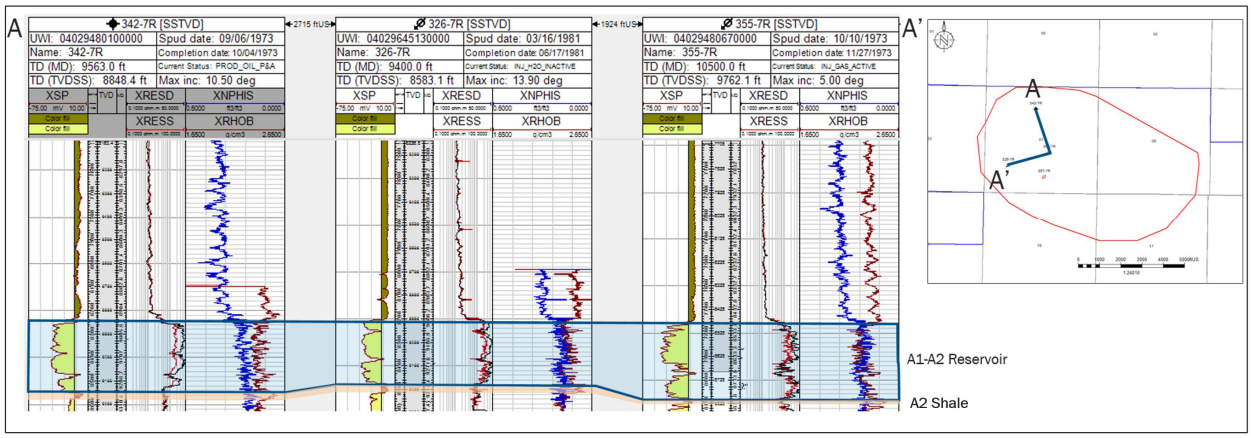

A key component of the A1-A2 reservoir characterization was the development of a geo-cellular model, which is used to assess CO_2 plume development through simulation and computational modeling studies. Results from the studies support plume size, structural and stratigraphic confinement, and storage capacity. A key input into the geo-cellular model is the characterization

of reservoir facies (sand versus shale). Cross-sections in Figures 38 and 39 shows the lateral continuity of the sand facies within the reservoir. Sand continuity and lack of internal baffles and barriers supports predictable plume development.

CO2 Injectate Confinement:

Confinement of CO_2 injected into the storage reservoir is supported by the following:

1. Prior to discovery of the Monterey Formation A1-A2 reservoir, a gas cap with underlying oil was confined for several million years.
2. The Reef Ridge Shale primary confining layer is 1,500 feet thick over the storage reservoir and has <0.01 mD permeability. Confinement of the Reef Ridge Shale has been demonstrated by the injection of 175 billion cubic feet of gas and five million barrels of water with no leakage.
3. Cross section A-A' (Figure 38) shows the lateral confinement of the injected CO_2 plume by the anticline structure. CTV plans to maintain the reservoir pressure at or beneath the discovery pressure of the reservoir, ensuring that CO_2 does migrate beyond the edges of the anticline structure or into the Reef Ridge shale.
4. In Cross section B-B' (Figure 39) the up-dip CO_2 plume is confined by shale and the non-deposition of reservoir sands.

Figure 38: Plume modeling results showing lateral confinement of the CO2 plume by the edges of the anticline structure 50 years post injection.

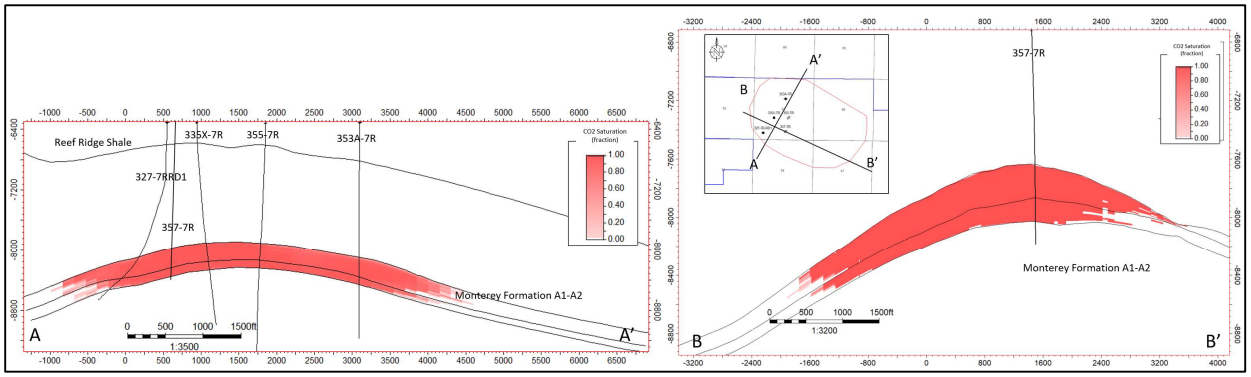

Figure 39: Plume modeling results showing the confinement of the plume against the up- dip pinch-out of the A1-A2 sand facies and the increasing shale facies.

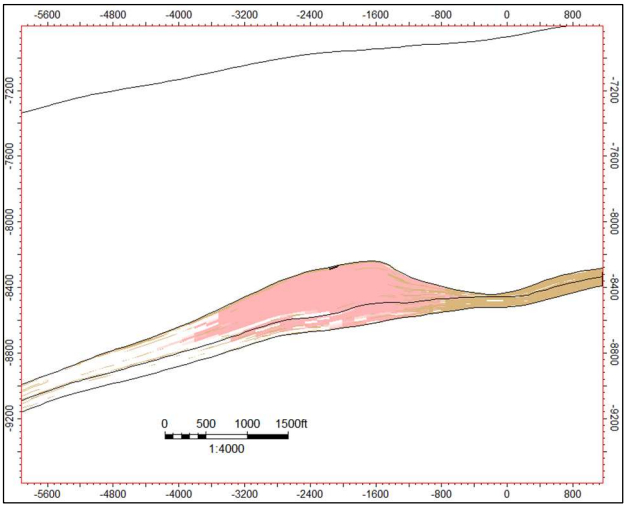

Storage capacity for the Monterey Formation A1-A2 storage reservoir based on computational modeling results is approximately 8 -10 million tonnes of CO_2. This is sufficient capacity for the total proposed injectate.

References:

1. Callaway, D.C., and Rennie, E.W., Jr., 1991, San Joaquin Basin, California, in Gluskoter, H.J., Rice, D.D., and Taylor, R. B., eds., Economic geology, U.S.: Boulder, Colorado, Geological Society of America, The Geology of North America, v. P-2, p. 417-430.
2. Zumberge, John, Russell, Just and Reid, Stephen, Charging of Elk Hills reservoirs as determined by oil geochemistry, AAPG Bulletin, v. 89, no. 10 (October 2005), pp. 1347–1371.
3. Hosford, Allegra and Magoon, Les, 2007 Age, U.S. Geological Survey Professional Paper 1713, California Petroleum Systems and Geologic Assessment of Oil and Gas in the San Joaquin Basin Province, California, Chapter 5.
4. Maher, J. C., R. D. Carter, and R. J. Lantz, 1975, Petroleum geology of naval petroleum reserve No. 1, Elk Hills, Kern County, California: U.S. Geological Survey Professional Paper 912, 109 p.
5. Castillo, David A. and Leland W. Younker. 1997. A High shear stress segment along the San Andreas Fault: Inferences based on near-field stress direction and stress magnitude observations in the Carrizo Plain Area.. United States: N. p., 1997. Web. doi:10.2172/490160.
6. Ingram, Gary and Urai, Janos. 1999. Top-seal leakage through faults and fractures: the role of mudrock properties. Geological Society, London, Special Publications. 158. 125-135. 10.1144/GSL.SP.1999.158.01.10.
7. Ingram G. M., Urai J. L., Naylor M. A. (1997) in Hydrocarbon Seals: Importance for Exploration and Production, Sealing processes and top seal assessment, Norwegian Petroleum Society (NPF) Special Publication, eds Moller-Pedersen P., Koestler A. G. **7**, pp 165–175.
8. Zhang, Jon & Yin, Shang-Xian. (2017). Fracture gradient prediction: an overview and an improved method. Petroleum Science. 14. 10.1007/s12182-017-0182-1.
9. Lacy, L., 1997, Dynamic Rock Mechanics Testing for Optimized Fracture Designs, SPE 38716, 1997 SPE Annual Technical Conference and Exhibition.
10. Yale, D.P. and Swami, V., 2017, Conversion of dynamic mechanical property calculations to static values for geomechanical modeling , presented at 51st US Rock Mechanics/ Geomechanics Symposium, San Francisco, June 2017. ARMA17-0644.
11. Fjaer, E., R.M. Holt, A.M. Raaen, and P. Horsrud. 2008. Petroleum related rock mechanics (2nd ed.). Elsevier Science.

Appendix – Core Data

Mineralogy for the Reef Ridge Shale confining layer from ten wells with core data. In the Core Type column, Conventional = whole core, PSWC = percussion sidewall core, and Cuttings = mudlog cuttings samples.

WELL	ANALYSIS METHOD	CORE TYPE	DEPTH (ft)	OPAL_A	OPAL_CT	CHERT	QUARTZ	PLAGIOCLASE	K_FELDSPARS	FELDSPAR	ALBITE	OLIGOCLASE	ANDESINE	CALCITE	DOLOMITE	PYRITE	CRYSTOBALITE	CLINOPTILOITE	BARITE STAR	ANALCIME	GYPSUM	SIDERITE	AMPHIBOLE	FLUORAPATITE	TOTAL CLAY	CHLORITE	KAOLINITE	ILLITE/MICA	SMECTITE	MIXED LAYER ILLITE/SMECTITE	% SMECTITE IN MXL I/S
355X-30R	FTIR	Conventional	5285.5	0	26	0	12		10		9	0	10	0	0	0	0								33	3	5			25	
355X-30R	FTIR	Conventional	5290	0	57	0	0		6		5	0	0	2	0	2	19								9	0	5			4	
355X-30R	FTIR	Conventional	5291.8	0	39	11	0		9		7	0	3	3	0	3	0								25	0	9			16	
355X-30R	FTIR	Conventional	5295.5	0	42	12	0		8		7	0	0	3	0	2	0								26	0	8			18	
355X-30R	FTIR	Conventional	5299.2	0	35	0	0		5		0	0	0	0	35	1	19								5	0	4			1	
355X-30R	FTIR	Conventional	5299.8	0	37	13	0		7		7	0	3	0	0	2	0								31	0	9			22	
355X-30R	FTIR	Conventional	5302.2	0	39	7	0		7		8	0	0	0	0	2	13								24	0	9			15	
355X-30R	FTIR	Conventional	5304.2	0	25	9	0		8		6	0	3	1	2	2	10								34	0	9			25	
355X-30R	FTIR	Conventional	5308.1	0	23	17	0		5		7	0	6	0	3	0	0								39	0	11			28	
355X-30R	FTIR	Conventional	5318	0	34	14	0		7		7	0	3	2	0	2	0								31	0	8			23	
355X-30R	FTIR	Conventional	5325	0	23	0	12		7		0	0	9	0	3	0	0								46	0	14			32	
355X-30R	FTIR	Conventional	5333	0	30	0	10		6		7	0	3	0	2	1	0								41	0	12			29	
355X-30R	FTIR	Conventional	5336.9	0	63	0	0		4		5	0	0	0	0	2	20								6	0	4			2	
355X-30R	FTIR	Conventional	5338.8	0	45	10	0		9		8	0	0	2	0	3	0								23	0	8			15	
355X-30R	FTIR	Conventional	5341.2	0	0	12	0		3		0	0	0	3	75	1	0								6	0	0			6	
355X-30R	FTIR	Conventional	5341.7	0	34	0	9		8		6	0	4	0	0	2	0								37	0	12			25	
355X-30R	FTIR	Conventional	5346.1	0	0	18	0		0		0	0	0	4	70	0	0								8	0	0			8	
355X-30R	FTIR	Conventional	5350.1	0	31	0	13		3		5	11	0	0	2	0	0								35	0	12			23	
355X-30R	FTIR	Conventional	5356	0	25	0	16		8		7	0	5	0	2	0	0								37	0	11			26	
355X-30R	FTIR	Conventional	5361.1	0	0	10	0		0		0	0	0	2	81	1	0								6	0	0			6	
355X-30R	FTIR	Conventional	5364.6	0	58	0	0		9		0	0	0	0	0	1	22								10	0	5			5	
355X-30R	FTIR	Conventional	5371	0	25	16	0		10		7	0	2	2	0	3	0								35	0	9			26	
355X-30R	FTIR	Conventional	5380.6	0	58	0	0		4		7	0	0	1	0	0	16								14	0	5			9	
355X-30R	FTIR	Conventional	5381	0	29	0	10		8		5	12	8	0	0	0	0								28	0	4			24	
355X-30R	FTIR	Conventional	5383.3	0	47	0	0		8		6	0	0	1	1	1	17								19	0	7			12	
355X-30R	FTIR	Conventional	5386.4	0	52	0	0		7		7	0	0	1	0	1	17								15	0	6			9	
355X-30R	FTIR	Conventional	5387.4	0	32	7	0		7		7	0	2	2	2	0	15								26	0	8			18	
355X-30R	FTIR	Conventional	5391.4	0	51	5	0		6		8	0	0	0	0	1	16								13	0	6			7	
355X-30R	FTIR	Conventional	5398.6	0	28	0	11		6		6	0	5	2	2	0	0								40	0	14			26	
355X-30R	FTIR	Conventional	5406.5	0	31	13	0		7		6	0	2	5	0	0	0								36	0	11			25	
355X-30R	FTIR	Conventional	5410.9	0	46	0	0		8		7	0	0	2	0	1	16								20	0	7			13	
355X-30R	FTIR	Conventional	5416.2	0	44	10	0		7		8	0	0	0	0	0	0								31	0	9			22	
355X-30R	FTIR	Conventional	5418.5	0	30	0	5		8		6	0	2	2	0	0	11								36	0	11			25	
355X-30R	FTIR	Conventional	5423.6	0	33	15	0		8		7	0	0	3	0	2	0								32	0	7			25	
355X-30R	FTIR	Conventional	5433.5	0	26	0	12		8		6	0	7	0	0	0	0								41	0	12			29	
355X-30R	FTIR	Conventional	5447.5	0	45	13	0		6		8	0	0	0	0	1	0								27	0	8			19	
58A-25R	FTIR	Conventional	4413.5		0	13	16		14		0	0	4	2	1	3	0								47	0	10			37	
58A-25R	FTIR	Conventional	4419.5		21	13	2		15		0	0	5	2	1	3	0								38	0	8			30	
58A-25R	FTIR	Conventional	4420.6		28	13	0		14		0	0	6	3	0	2	0								34	0	8			26	
58A-25R	FTIR	Conventional	4424.5		18	0	15		14		0	0	6	2	0	4	0								41	0	10			31	
58A-25R	FTIR	Conventional	4432.5		20	0	13		12		0	0	5	1	1	3	0								45	0	11			34	
58A-25R	FTIR	Conventional	4438.4		57	0	0		9		0	0	0	0	0	0	20								14	5	4			5	
58A-25R	FTIR	Conventional	4439.5		47	0	0		12		0	0	0	0	0	2	21								18	6	7			5	
58A-25R	FTIR	Conventional	4443.4		37	0	0		12		0	0	0	0	8	2	22								19	5	7			7	
58A-25R	FTIR	Conventional	4447.8		47	0	0		11		0	0	0	1	1	0	21								19	4	6			9	
58A-25R	FTIR	Conventional	4452.4		34	15	0		12		0	0	2	0	0	3	0								34	0	10			24	
58A-25R	FTIR	Conventional	4460.5		23	17	0		12		0	0	3	3	2	2	0								38	0	11			27	
58A-25R	FTIR	Conventional	4468.5		0	19	13		13		0	0	0	3	2	2	0								48	0	13			35	
58A-25R	FTIR	Conventional	4469.5		0	19	13		11		5	0	0	3	3	2	0								44	0	12			32	
58A-25R	FTIR	Conventional	4476.5		31	0	0		13		0	0	5	2	0	2	15								32	0	8			24	
58A-25R	FTIR	Conventional	4480.5		42	0	0		13		0	0	0	0	0	1	22								22	5	9			8	
58A-25R	FTIR	Conventional	4481.6		43	0	0		11		0	0	0	0	0	2	22								22	5	7			10	
58A-25R	FTIR	Conventional	4486.5		34	0	0		12		0	0	5	2	0	2	16								29	0	8			21	
58A-25R	FTIR	Conventional	4490.5		29	13	0		14		0	0	6	0	0	5	0								33	0	7			26	

58A-25R	FTIR	Conventional	4492.6		53	0	0		8		0	0	0	0	0	2	22								15	7	6			2	
58A-25R	FTIR	Conventional	4497.9		48	0	0		10		0	0	0	1	0	1	23								17	6	6			5	
58A-25R	FTIR	Conventional	4498.4		37	5	0		12		0	0	0	2	0	1	18								25	6	7			12	
58A-25R	FTIR	Conventional	4499.5		41	0	0		10		0	0	0	2	0	2	22								23	6	7			10	
328-28R	FTIR	Conventional	5049.8		36	1	2	0	1		8			0	0	2	20								20	0	6			14	
328-28R	FTIR	Conventional	5052.9	0	28	0	0		11		0	7	0	0	0	0	17								37	4	11			22	
328-28R	FTIR	Conventional	5070		34	4	2	0	1		4			0	0	2	19								24	0	3			21	
328-28R	FTIR	Conventional	5070.3	0	43	0	0		6		5	0	0	0	0	0	22								24	4	6			14	
328-28R	FTIR	Conventional	5070.5	0	37	0	0		12		0	0	0	0	0	0	23								28	4	7			17	
328-28R	FTIR	Conventional	5085.4		32	4	2	9	8		4			0	0	0	14								27	0	9			18	
368H-19R	FTIR	Conventional	4800.5	0	25	8	10		13		7	0	2	0	0	2	0								33	0	7			26	
368H-19R	FTIR	Conventional	4801.5	0	46	0	0		8		5	0	0	0	0	3	18								20	0	6			14	
368H-19R	FTIR	Conventional	4802.5	0	36	11	0		10		7	0	0	1	0	3	0								32	0	8			24	
368H-19R	FTIR	Conventional	4804.5	0	32	0	11		11		5	0	1	1	0	2	0								37	0	9			28	
368H-19R	FTIR	Conventional	4810.5	0	35	10	0		10		7	0	0	0	0	3	0								35	0	7			28	
368H-19R	FTIR	Conventional	4813.5	0	35	6	0		10		7	0	1	2	0	1	12								26	0	7			19	
368H-19R	FTIR	Conventional	4819.5	0	39	0	0		11		6	0	3	2	0	2	15								22	0	6			16	
368H-19R	FTIR	Conventional	4823.5	0	46	0	0		8		6	0	0	3	0	2	18								17	0	7			10	
368H-19R	FTIR	Conventional	4824.5	0	31	11	0		11		7	0	0	0	0	4	0								36	0	7			29	
368H-19R	FTIR	Conventional	4834.5	0	21	0	13		13		4	0	3	0	1	3	0								42	0	9			33	
368H-19R	FTIR	Conventional	4837.5	0	0	0	0		6		0	0	4	8	73	1	0								8	0	0			8	
368H-19R	FTIR	Conventional	4842.5	0	21	0	13		15		0	0	6	2	0	3	0								40	0	9			31	
368H-19R	FTIR	Conventional	4852.5	0	26	0	11		12		4	0	4	3	0	3	0								37	0	8			29	
368H-19R	FTIR	Conventional	4858.5	0	41	0	0		10		6	0	3	1	0	2	17								20	0	7			13	
368H-19R	FTIR	Conventional	4860.4	0	16	6	0		3		0	0	1	0	66	1	0								7	0	0			7	
368H-19R	FTIR	Conventional	5000.5	0	29	8	0		13		4	0	4	0	6	3	0								33	0	9			24	
368H-19R	FTIR	Conventional	5004.5	0	0	0	0		0		0	0	1	0	83	0	0								16	0	0			16	
368H-19R	FTIR	Conventional	5010.5	0	34	10	0		13		0	0	0	2	0	3	0								38	0	10			28	
368H-19R	FTIR	Conventional	5016.5	0	22	10	4		13		0	0	3	3	0	3	0								42	0	10			32	
368H-19R	FTIR	Conventional	5020.5	0	19	14	4		16		0	0	0	4	1	3	0								39	0	8			31	
368H-19R	FTIR	Conventional	5025.5	0	25	13	0		12		5	0	0	2	0	3	0								40	0	8			32	
368H-19R	FTIR	Conventional	5028.5	0	35	0	0		11		4	0	3	4	2	1	18								22	0	7			15	
368H-19R	FTIR	Conventional	5035.5	0	50	0	0		8		5	0	0	1	0	2	25								9	0	6			3	
368H-19R	FTIR	Conventional	5036.5	0	41	0	0		11		4	0	2	0	0	2	23								17	0	7			10	
368H-19R	FTIR	Conventional	5038.5	0	38	9	0		10		5	0	3	2	0	2	0								31	0	8			23	
368H-19R	FTIR	Conventional	5042.5	0	47	0	0		7		6	0	0	1	0	1	23								15	0	7			8	
368H-19R	FTIR	Conventional	5047.5	0	38	0	0		12		0	0	0	2	0	2	18								28	0	7			21	
368H-19R	FTIR	Conventional	5052.5	0	35	0	0		13		0	0	3	1	0	2	17								29	0	9			20	
368H-19R	FTIR	Conventional	5056.5	0	35	0	0		11		4	0	3	2	2	1	16								26	0	8			18	
368H-19R	FTIR	Conventional	5059.6	0	0	10	0		0		0	0	0	7	76	0	0								7	0	0			7	
368H-19R	FTIR	PSWC	4677		54	0	0		9		8	0	2	1	0	1	14								11	0	4			7	
368H-19R	FTIR	PSWC	4714		34	9	0		9		7	0	4	2	0	2	0								33	0	7			26	
368H-19R	FTIR	PSWC	4722		47	0	0		9		8	0	2	1	0	2	15								16	0	6			10	
368H-19R	FTIR	PSWC	4746		40	10	0		8		7	0	0	3	0	2	0								30	0	7			23	
368H-19R	FTIR	PSWC	4862		33	8	0		11		5	0	8	0	0	4	0								31	0	7			24	
368H-19R	FTIR	PSWC	4866		44	0	0		8		6	0	1	0	2	3	17								19	0	7			12	
368H-19R	FTIR	PSWC	5105		45	10	0		7		7	0	0	0	0	1	0								30	0	7			23	
368H-19R	FTIR	PSWC	5130		36	0	0		10		5	0	2	0	0	2	18								27	0	7			20	
382XH-36R	FTIR	Cuttings	4107	0	42	6	0		11		9	0	9	2	0	2	0								19	0	6			13	
382XH-36R	FTIR	Cuttings	4240	0	41	0	0		10		7	0	5	0	2	1	13								21	0	6			15	
382XH-36R	FTIR	Cuttings	4400	0	50	0	0		9		7	0	2	0	0	2	17								13	0	7			6	
382XH-36R	FTIR	Cuttings	4466	0	44	0	0		11		0	0	3	2	0	0	20								20	0	5			15	
365-24Z	XRD	Conventional	4154.6		72		7	7	1					0	0	3		0		0	1	0		0	9						
365-24Z	XRD	Conventional	4160.5		71		8	6	2					0	0	4		0		0	1	0		0	8						
365-24Z	XRD	Conventional	4162		24		17	16	3					0	0	9		0		0	4	0		0	27						
365-24Z	XRD	Conventional	4162.5		50		12	9	2					0	0	6		1		0	3	0		0	17						
365-24Z	XRD	Conventional	4163.4		64		13	7	2					0	0	3		0		0	1	0		0	10						
365-24Z	XRD	Conventional	4163.5		61		10	10	3					0	0	4		0		0	0	0		0	12						
365-24Z	XRD	Conventional	4172.5		56		10	9	2					0	0	4		0		0	1	0		0	18						
365-24Z	XRD	Conventional	4176.4		71		6	7	1					0	0	3		1		0	0	0		0	11						
365-24Z	XRD	Conventional	4522.5		67		11	7	1					0	0	4		0		0	0	0		1	9						
365-24Z	XRD	Conventional	4523.5		72		10	5	2					0	0	3		0		0	0	0		1	7						
365-24Z	XRD	Conventional	4555.5		47		17	8	2					0	0	4		1		0	0	0		1	20						
348AH-31S	FTIR	Conventional	4494.75	0	49	0	0		8		10	0	0	2	0	2	15								14	3	6			5	
348AH-31S	FTIR	Conventional	4496.25	0	46	0	0		11		8	0	0	1	0	2	18								14	3	7			4	
348AH-31S	FTIR	Conventional	4497.75	0	65	0	0		9		8	0	5	1	0	1	0								11	0	6			5	
348AH-31S	FTIR	Conventional	4499.25	0	55	7	0		8		9	0	3	2	0	2	0								14	0	7			7	
348AH-31S	FTIR	Conventional	4500.5	0	37	12	0		13		7	0	7	3	0	2	0								19	0	6			13	
348AH-31S	FTIR	Conventional	4501.2	0	35	11	0		12		0	0	3	4	21	1	0								13	0	4			9	
348AH-31S	FTIR	Conventional	4502.2	0	42	9	0		11		8	0	6	0	3	1	0								20	0	7			13	
348AH-31S	FTIR	Conventional	4503.55	0	43	10	0		11		7	0	5	0	1	1	0								22	0	8			14	
348AH-31S	FTIR	Conventional	4504.6	0	68	0	0		9		8	0	3	0	0	0	0								12	0	5			7	
348AH-31S	FTIR	Conventional	4505.55	0	0	14	0		0		0	0	0	10	69	0	0								7	0	0			7	

348AH-31S	FTIR	Conventional	4507	0	43	0	0		13		7	0	3	0	0	2	18								14	0	7			7	
348AH-31S	FTIR	Conventional	4508.65	0	44	8	0		12		8	0	6	2	0	2	0								18	0	6			12	
348AH-31S	FTIR	Conventional	4509.65	0	46	8	0		9		7	0	3	0	11	2	0								14	0	6			8	
348AH-31S	FTIR	Conventional	4510.5	0	44	0	0		11		8	0	3	0	1	2	15								16	0	6			10	
348AH-31S	FTIR	Conventional	4511.6	0	43	0	0		13		6	0	3	0	0	2	15								18	0	6			12	
348AH-31S	FTIR	Conventional	4512.75	0	63	0	0		10		8	0	4	0	0	0	0								15	0	3			12	
348AH-31S	FTIR	Conventional	4513.65	0	51	0	4		17		0	0	0	0	0	0	0								28	0	0			28	
348AH-31S	FTIR	Conventional	4964.25	0	43	0	0		11		6	0	4	0	0	2	13								21	0	6			15	
348AH-31S	FTIR	Conventional	4515.5	0	48	0	0		12		0	0	6	0	0	0	15								19	0	4			15	
348AH-31S	FTIR	Conventional	4517.25	0	39	0	0		12		6	0	2	0	0	2	16								23	3	8			12	
348AH-31S	FTIR	Conventional	4518.75	0	42	9	0		14		0	0	8	0	0	0	0								27	0	5			22	
348AH-31S	FTIR	Conventional	4519.75	0	50	0	0		12		7	0	11	2	0	1	0								17	0	5			12	
348AH-31S	FTIR	Conventional	4520.5	0	43	0	0		13		8	0	0	1	0	2	17								16	4	7			5	
348AH-31S	FTIR	Conventional	4521.5	0	46	10	0		12		10	0	7	0	0	2	0								13	0	5			8	
348AH-31S	FTIR	Conventional	4522.35	0	39	10	0		10		8	0	7	2	0	2	0								22	0	7			15	
348AH-31S	FTIR	Conventional	4523.1	0	55	0	0		10		6	0	9	0	0	1	0								19	0	6			13	
348AH-31S	FTIR	Conventional	5017.5	0	17	37	4		10		0	0	6	0	0	2	0								24	0	7			17	
348AH-31S	FTIR	Conventional	5018.25	0	0	42	0		10		0	0	4	0	0	2	22								20	0	6			14	
348AH-31S	FTIR	Conventional	5018.75	0	12	38	0		10		0	0	3	2	0	1	14								20	0	5			15	
348AH-31S	FTIR	Conventional	5019.25	0	13	38	0		9		0	0	3	2	0	1	13								21	0	5			16	
348AH-31S	FTIR	Conventional	5019.6	0	0	48	0		9		0	0	6	3	0	2	0								32	0	7			25	
348AH-31S	FTIR	Conventional	5019.95	0	19	40	5		10		0	0	2	0	2	1	0								21	0	5			16	
348AH-31S	FTIR	Conventional	5020.5	0	0	49	7		10		0	0	4	2	0	2	0								26	0	6			20	
348AH-31S	FTIR	Conventional	5021.35	0	0	55	3		9		0	0	3	0	2	2	0								26	0	5			21	
348AH-31S	FTIR	Conventional	5022.2	0	0	55	0		7		0	0	3	2	1	1	0								31	0	6			25	
348AH-31S	FTIR	Conventional	5022.75	0	0	40	6		9		0	0	3	1	1	1	12								27	0	6			21	
348AH-31S	FTIR	Conventional	5023.4	0	0	41	0		9		0	0	0	2	0	2	19								27	3	7			17	
348AH-31S	FTIR	Conventional	5024	0	0	46	4		9		0	0	4	3	0	2	0								32	0	8			24	
348AH-31S	FTIR	Conventional	5024.45	0	0	54	4		10		0	0	2	2	0	2	0								26	0	5			21	
348AH-31S	FTIR	Conventional	5024.85	0	0	51	2		9		0	0	2	3	0	2	0								31	0	7			24	
348AH-31S	FTIR	Conventional	5025.3	0	0	53	4		8		0	0	3	2	1	1	0								28	0	6			22	
348AH-31S	FTIR	Conventional	5026.2	0	0	54	2		9		0	0	2	3	0	2	0								28	0	6			22	
348AH-31S	FTIR	Conventional	5027.2	0	0	45	9		9		0	0	3	3	0	2	0								29	0	6			23	
348AH-31S	FTIR	Conventional	5027.8	0	0	43	4		10		0	0	3	4	0	2	0								34	0	8			26	
348AH-31S	FTIR	Conventional	5028.75	0	0	49	2		8		0	0	3	2	1	1	0								34	0	8			26	
348AH-31S	FTIR	Conventional	5029.6	0	0	49	1		9		0	0	2	2	1	2	0								34	0	7			27	
348AH-31S	FTIR	Conventional	5030.1	0	11	39	4		8		0	0	1	2	2	1	0								32	0	6			26	
348AH-31S	FTIR	Conventional	5030.85	0	0	53	0		8		0	0	2	3	0	1	0								33	0	8			25	
348AH-31S	FTIR	Conventional	5031.8	0	0	53	0		8		0	0	0	4	0	1	0								34	0	9			25	
348AH-31S	FTIR	Conventional	5032.7	0	0	49	0		8		0	0	4	3	2	1	0								33	0	8			25	
348AH-31S	FTIR	Conventional	5033.65	0	0	48	0		8		0	0	4	4	0	1	0								35	0	9			26	
348AH-31S	FTIR	Conventional	5034.6	0	0	44	0		9		0	0	2	3	2	1	0								39	0	10			29	
348AH-31S	FTIR	Conventional	5035.5	0	0	43	0		9		0	0	0	3	2	1	0								42	0	11			31	
348AH-31S	FTIR	Conventional	5036.3	0	0	41	0		9		0	0	0	3	2	1	0								44	0	12			32	
348AH-31S	FTIR	Conventional	5036.8	0	0	40	0		9		0	0	2	4	2	1	0								42	0	12			30	
348AH-31S	FTIR	Conventional	5037.25	0	0	42	0		8		0	0	0	4	2	1	0								43	0	12			31	
348AH-31S	FTIR	Conventional	5037.75	0	0	42	0		7		0	0	0	3	1	3	0								44	0	13			31	
348AH-31S	FTIR	Conventional	5038.8	0	0	41	0		10		0	0	0	3	2	2	0								42	0	12			30	
348AH-31S	FTIR	Conventional	5040.25	0	0	43	0		8		0	0	0	2	1	2	0								44	0	13			31	
348AH-31S	FTIR	Conventional	5041.5	0	0	44	0		9		0	0	0	2	1	2	0								42	0	12			30	
348AH-31S	FTIR	Conventional	5043	0	0	40	0		10		0	0	0	2	1	2	0								45	0	11			34	
348AH-31S	FTIR	Conventional	5044.45	0	0	47	0		9		0	0	0	3	0	2	0								39	0	10			29	
348AH-31S	FTIR	Conventional	5045.55	0	0	47	0		10		0	0	0	2	1	1	0								39	0	10			29	
348AH-31S	FTIR	Conventional	5046.85	0	0	51	0		11		0	0	0	2	0	1	0								35	0	10			25	
348AH-31S	FTIR	Conventional	5047.85	0	0	51	0		9		0	0	2	0	0	3	0								35	0	9			26	
348AH-31S	FTIR	Conventional	5048.5	0	0	57	0		10		0	0	0	2	0	2	0								29	0	8			21	
348AH-31S	FTIR	Conventional	5049	0	0	49	0		10		0	0	0	2	3	2	0								34	0	9			25	
348AH-31S	FTIR	Conventional	5049.6	0	0	17	0		0		0	0	0	14	58	0	0								11	0	0			11	
348AH-31S	FTIR	Conventional	5050.5	0	0	57	0		8		0	0	0	0	2	1	0								32	0	9			23	
348AH-31S	FTIR	Conventional	5051.4	0	0	55	0		8		0	0	2	0	1	1	0								33	0	9			24	
348AH-31S	FTIR	Conventional	5052.15	0	0	60	0		7		0	0	2	0	2	1	0								28	0	7			21	
348AH-31S	FTIR	Conventional	5052.6	0	0	50	0		10		0	0	5	2	0	1	0								32	0	9			23	
348AH-31S	FTIR	Conventional	5052.9	0	0	53	0		8		0	0	0	2	0	1	11								25	0	7			18	
348AH-31S	FTIR	Conventional	5053.2	0	0	56	0		9		0	0	4	3	0	1	0								27	0	8			19	
348AH-31S	FTIR	Conventional	5053.9	0	0	62	0		7		0	0	0	2	0	2	0								27	0	7			20	
348AH-31S	FTIR	Conventional	5054.95	0	0	54	0		7		0	0	0	2	0	1	11								25	3	6			16	
348AH-31S	FTIR	Conventional	5055.45	0	0	54	0		8		0	0	0	2	1	2	0								33	2	8			23	
348AH-31S	FTIR	Conventional	5056	0	0	67	0		8		0	0	3	2	0	1	0								19	0	5			14	
348AH-31S	FTIR	Conventional	5056.9	0	0	55	0		9		0	0	0	3	0	1	11								21	0	5			16	
348AH-31S	FTIR	Conventional	5057.55	0	0	51	0		11		0	0	6	3	0	2	0								27	0	6			21	
348AH-31S	FTIR	Conventional	5058.05	0	0	59	0		2		0	0	0	2	0	3	0								34	3	7			24	
348AH-31S	FTIR	Conventional	5058.6	0	0	53	0		9		0	0	3	3	0	2	0								30	0	8			22	
348AH-31S	FTIR	Conventional	5059.55	0	0	57	0		8		0	0	3	3	0	1	0								28	0	7			21	

348AH-31S	FTIR	Conventional	5060.5	0	0	48	0		8		0	0	0	2	0	1	10								31	3	7			21	
348AH-31S	FTIR	Conventional	5061.15	0	0	63	0		0		0	0	0	3	0	0	0								34	3	4			27	
348AH-31S	FTIR	Conventional	5061.6	0	0	55	0		8		0	0	3	3	0	1	0								30	0	7			23	
348AH-31S	FTIR	Conventional	5062.1	0	0	64	0		8		0	0	0	2	0	1	0								25	0	6			19	
348AH-31S	FTIR	Conventional	5062.95	0	0	57	0		9		0	0	4	2	0	1	0								27	0	6			21	
348AH-31S	FTIR	Conventional	5063.95	0	0	63	0		8		0	0	4	1	3	1	0								20	0	3			17	
348AH-31S	FTIR	Conventional	5064.65	0	0	55	0		6		3	0	3	3	7	1	0								22	0	4			18	
348AH-31S	FTIR	Conventional	5065.15	0	0	52	0		7		0	0	0	3	7	2	10								19	3	3			13	
348AH-31S	FTIR	Conventional	5065.85	0	0	54	0		7		0	0	3	4	11	1	0								20	0	5			15	
368AH-32S	XRD	PSWC	4931		9		32	19	1					0	0	2			0			0			37	0	1.85	14.43	20.72		
368AH-32S	XRD	PSWC	5070		15		39	10	0					0	0	2			0			2			32	0	1.28	12.8	17.92		
368AH-32S	XRD	PSWC	5136		21		36	9	0					0	2	2			0			1			29	0	0.87	13.63	14.5		
368AH-32S	XRD	PSWC	5186		0		8	1	0					0	88	0			0			0			3	0	0.21	1.92	0.87		
368AH-32S	XRD	PSWC	5224		0		8	1	0					0	81	1			0			0			9	0	1.17	2.97	4.86		
368AH-32S	XRD	PSWC	5234		18		44	8	0					0	1	2			0			2			25	0	1.75	10.25	13		
368AH-32S	XRD	PSWC	5375		20		39	7	0					0	0	2			0			2			30	0	0.6	12.6	16.8		
368AH-32S	XRD	PSWC	5419		0		53	6	0					1	1	2			0			3			34	0	2.38	8.5	23.12		
368AH-32S	XRD	PSWC	5438		0		52	9	0						4	2			0			2			31	0	0.93	9.61	20.46		
353X-24Z	FTIR	Cuttings	3971		70	0	0		4		0	0	0	0	0	0	13								13	3	0			10	
353X-24Z	FTIR	Cuttings	3982		43	0	0		12		0	0	0	0	0	2	12								31	5	6			20	
353X-24Z	FTIR	Cuttings	3992		61	0	0		6		7	0	3	1	0	0	0								22	0	4			18	
353X-24Z	FTIR	Cuttings	4108		30	0	12		15		8	0	7	0	0	2	0								26	0	6			20	
353X-24Z	FTIR	Cuttings	4115		32	0	17		14		9	0	6	0	0	2	0								20	0	4			16	
353X-24Z	FTIR	Cuttings	4174		33	0	8		12		6	0	7	0	0	3	0								31	0	7			24	
353X-24Z	FTIR	Cuttings	4282		61	0	0		6		5	0	0	0	0	2	15								11	2	5			4	
353X-24Z	FTIR	Cuttings	4286		55	0	0		12		0	0	0	0	0	2	16								15	3	4			8	
353X-24Z	FTIR	Cuttings	4309		53	0	4		7		7	0	4	0	0	2	0								23	0	7			16	
353X-24Z	FTIR	Cuttings	4351		19	0	13		13		0	0	4	0	5	1	0								45	0	11			34	
353X-24Z	FTIR	Cuttings	4360		58	0	0		6		0	0	0	0	0	0	16								20	7	3			10	
353X-24Z	FTIR	Cuttings	4365		45	0	0		5		0	0	0	0	25	0	13								12	4	1			7	
353X-24Z	FTIR	Cuttings	4416		44	0	0		10		6	0	0	2	0	2	16								20	4	7			9	
353X-24Z	FTIR	Cuttings	4421		52	0	0		6		0	10	0	0	0	0	15								17	3	2			12	
353X-24Z	FTIR	Cuttings	4426		47	0	0		8		0	0	0	10	6	0	17								12	5	4			3	
353X-24Z	FTIR	Cuttings	4526		39	0	0		10		5	0	3	2	0	0	18								23	0	5			18	
353X-24Z	FTIR	Cuttings	4548		45	0	0		9		5	0	0	1	0	2	19								19	5	6			8	
353X-24Z	FTIR	Cuttings	4558		32	0	0		14		0	0	7	5	0	0	15								27	0	4			23	
353X-24Z	FTIR	Cuttings	4605		45	0	0		10		0	0	0	2	0	0	21								22	5	4			13	
66-29R	XRD	Conventional	4612.4		34		22	11	5						0	3		0				2	0	0	23	0.7	1.2	6.2		15	80-90
66-29R	XRD	Conventional	4653.5		41		19	9	2						0	4		0				2	0	0	23	0.7	0.9	6.7		14.7	80-90
66-29R	XRD	Conventional	4668.55		25		22	12	3						0	5		0				1	0	0	32	1.3	1.9	7.7		21.1	80-90
66-29R	XRD	Conventional	4676.1		35		18	10	3						0	4		0				3	0	0	27	1.1	1.9	7.3		16.7	80-90

Mercury injection capillary pressure (MICP) derived core porosity and permeability from 13 wells with 175 data points in the Monterey Formation.

WELL NAME	DEPTH (MD feet)	MICP Permeability (mD)	MICP Porosity (%)	Lithology
317-8R	8865	160	24	Sand
317-8R	8868	58	20.7	Sand
317-8R	8869	13	18.7	Sand
317-8R	8948	39	17	Sand
317-8R	8952	50	17.9	Sand
317-8R	8960	37	16.5	Sand
317-8R	8971	19	17.2	Sand
317-8R	8974	75	20.1	Sand
322-31S	5932.2	0.526	20.1	Non-Reservoir
322-31S	5935.2	0.933	23.1	Non-Reservoir
322-31S	5935.5	0.466	17.4	Non-Reservoir
322-31S	5936.6	1.06	22	Non-Reservoir
322-31S	5936.7	0.236	16.4	Non-Reservoir
322-31S	5936.9	0.0278	11.1	Non-Reservoir
322-31S	5937.5	0.0176	10.5	Non-Reservoir
322-31S	5937.9	1.22	27.7	Non-Reservoir
328A-32S	5250.4	0.0053	18.2	Non-Reservoir
328A-32S	5252.6	0.0731	23.2	Non-Reservoir
328A-32S	5256.7	0.0684	35.8	Non-Reservoir
328A-32S	5257.5	0.0012	13.6	Non-Reservoir
328A-32S	5258.5	0.0366	31.4	Non-Reservoir
328A-32S	5259.5	0.0512	42.1	Non-Reservoir
328A-32S	5261.4	3.89	40.4	Non-Reservoir
328A-32S	5262.5	2.03	32.5	Non-Reservoir
328A-32S	5267	0.188	24.3	Non-Reservoir
328A-32S	5267.4	0.0013	12.5	Non-Reservoir
328A-32S	5272.5	0.112	17.6	Non-Reservoir
334-36S	8031.9	21	14.76	Sand
334-36S	8058.5	18	16.08	Sand
334-36S	8069.75	2.36	16.29	Sand
334-36S	8071.15	19.1	18.53	Sand
334-36S	8092.55	7.89	13.64	Sand
334-36S	8098.6	7.39	18.24	Sand
334-36S	8102.6	14.2	15.58	Sand
334-36S	8104.5	20.9	13.88	Sand
344-4G	6519.4	0.112	16.2	Non-Reservoir
344-4G	6520	0.074	15	Non-Reservoir
344-4G	6522.9	0.049	15.5	Non-Reservoir
344-4G	6524.1	0.084	16.1	Non-Reservoir
344-4G	6526.6	0.044	13.9	Non-Reservoir
344-4G	6530.7	0.091	15.3	Non-Reservoir
344-4G	6533.2	0.025	15.9	Non-Reservoir
344-4G	6552	0.03	12.9	Non-Reservoir
344-4G	6553.4	0.023	15	Non-Reservoir
344-4G	6557.3	0.0004	10.4	Non-Reservoir
344-4G	6559.1	0.0086	14.4	Non-Reservoir
344-4G	6574.6	0.00043	9.59	Non-Reservoir
344-4G	6575.4	0.151	14.8	Non-Reservoir
344-4G	6585.7	0.00028	7.45	Non-Reservoir
344-4G	6586.7	0.0102	13.2	Non-Reservoir
344-4G	6587.9	0	0.05	Non-Reservoir
344-4G	6868.9	0.284	11	Sand
344-4G	6869.5	0.176	9.73	Sand
344-4G	6878.5	0.00044	8.38	Non-Reservoir
344-4G	6909.6	2.48	15	Sand
344-4G	6920.6	0.15	10.8	Sand
344-4G	6943.3	1.98	16	Sand
344-4G	6943.9	2.35	15.4	Sand
344-4G	6990.7	0.043	15.8	Non-Reservoir
344-4G	7001.7	0.0028	9.55	Non-Reservoir
344-4G	7016.8	0.0046	7.01	Non-Reservoir
344-4G	7022.5	0.0386	12	Non-Reservoir
344-4G	7033.7	0.0135	14.6	Non-Reservoir
347X-36S	9348.5	0.902	8.83	Sand
347X-36S	9359.8	0.0082	8.29	Non-Reservoir
347X-36S	9361.1	0.002	9.29	Non-Reservoir
347X-36S	9361.5	0.0055	10.1	Non-Reservoir
347X-36S	9363.7	0.0032	8.74	Non-Reservoir
347X-36S	9364.75	9.67	12.5	Sand
347X-36S	9366.1	0.556	12	Sand
347X-36S	9369.4	0.0148	9.67	Non-Reservoir
347X-36S	9369.4	0.009	9.63	Non-Reservoir
347X-36S	9369.8	0.0263	11.5	Non-Reservoir
347X-36S	9426.4	0.017	23.5	Non-Reservoir
347X-36S	9436	0.0066	7.83	Non-Reservoir
347X-36S	9452	1.75	10.2	Sand
347X-36S	9452.45	0.563	9.19	Sand
347X-36S	9453	0.484	10.6	Sand
347X-36S	9547.4	0.0028	8.55	Non-Reservoir
347X-36S	9547.6	0.00095	6.95	Non-Reservoir
347X-36S	9552	0.0174	5.38	Sand
352A-25R	6255.6	0.886	19.1	Non-Reservoir
352A-25R	6263.4	0.00012	7.02	Non-Reservoir
352A-25R	6282.6	0.325	18.3	Non-Reservoir
352A-25R	6290.5	1.58	26.6	Non-Reservoir
352A-25R	6294.2	1.57	25.5	Non-Reservoir
352A-25R	6299.6	0.00086	8.67	Non-Reservoir
356XH-25R	5510	0.0074	19.95	Non-Reservoir
356XH-25R	5510.1	0.0101	14.51	Non-Reservoir
356XH-25R	5524.4	0.0471	16.97	Non-Reservoir
356XH-25R	5534.1	1.479	33.39	Non-Reservoir
356XH-25R	5541	0.0422	39.81	Non-Reservoir
358-23R	5780.5	0.279	20.7	Non-Reservoir
358-23R	5785.5	0.312	14.4	Non-Reservoir
358-23R	5792.5	0.626	23.7	Non-Reservoir
358-23R	5796.5	0.0617	16.3	Non-Reservoir
358-23R	5801.5	0.05	16.7	Non-Reservoir
358-23R	5803.5	0.111	17.5	Non-Reservoir
358-23R	5805.5	0.442	21.3	Non-Reservoir
358-23R	5811.5	0.00571	14.3	Non-Reservoir
358-23R	5813.5	0.0216	17.3	Non-Reservoir
358-23R	5816.5	0.0534	20.3	Non-Reservoir
358-23R	5820.5	0.0105	15.4	Non-Reservoir
358-23R	5829.5	0.0117	16.7	Non-Reservoir
358-23R	5864.5	2.05	34.4	Non-Reservoir
363X-16R	8603.7	0.0173	6.97	Sand
363X-16R	8642.8	0.0246	5.47	Sand
363X-16R	8653.9	0.048	3.25	Sand
363X-16R	8655.4	0.00605	10.1	Non-Reservoir
363X-16R	8662.6	7.2	6.92	Sand
363X-16R	8666.6	0.0154	10.2	Non-Reservoir
363X-16R	8667.3	0.0088	9.68	Non-Reservoir
363X-16R	8680.9	0.00072	1.34	Non-Reservoir
363X-16R	8993.1	0.598	10.2	Sand
363X-16R	8996.9	0.592	12.1	Sand
363X-16R	9001.45	2.85	14.1	Sand
363X-16R	9004.7	2.59	13	Sand
363X-16R	9015.5	12.6	16.7	Sand
363X-16R	9016.6	9.65	16	Non-Reservoir
363X-16R	9027.1	1.17	10.9	Sand
363X-16R	9028.5	2.44	12.6	Sand
363X-16R	9035.8	2.75	13.2	Sand
363X-16R	9044.5	1.39	11.9	Sand
363X-16R	9059.4	12.6	10.9	Sand
363X-16R	9072.8	0.151	11.5	Sand
363X-16R	9093.5	0.216	8.29	Sand
365-24Z	3704.5	0.00138	16.9	Non-Reservoir
365-24Z	3748.5	0.00309	19.3	Non-Reservoir
365-24Z	3774.5	0.00251	19.3	Non-Reservoir
365-24Z	3815.5	0.00087	17.3	Non-Reservoir
365-24Z	4107.5	0.00022	11.9	Non-Reservoir
365-24Z	4110.5	0.00036	14.2	Non-Reservoir
365-24Z	4154.6	0.0003	13.6	Non-Reservoir
365-24Z	4160.5	0.00039	16.3	Non-Reservoir
365-24Z	4162	0.00056	16.6	Non-Reservoir
365-24Z	4162.5	0.00019	10.8	Non-Reservoir
365-24Z	4163.4	0.00012	8.27	Non-Reservoir
365-24Z	4163.5	0.00017	9.76	Non-Reservoir
365-24Z	4172.5	0.00014	8.88	Non-Reservoir
365-24Z	4176.4	0.00015	9.21	Non-Reservoir
365-24Z	4523.5	0.00033	14.2	Non-Reservoir
365-24Z	4527.5	0.00028	12.9	Non-Reservoir
365-24Z	4555.5	0.00026	12.3	Non-Reservoir
375-36R	5423.9	0.00103	13.7	Non-Reservoir
375-36R	5432.6	0.314	25.7	Non-Reservoir
375-36R	5451.4	0.679	30.1	Non-Reservoir
375-36R	5461.1	0.0861	19.1	Non-Reservoir
375-36R	5479.4	2.46	32	Non-Reservoir
375-36R	5480.9	1.5	30.9	Non-Reservoir
375-36R	5754.6	60.4	18.2	Sand
375-36R	5763.9	0.7	13.2	Sand
375-36R	5765.9	0.0297	20.8	Non-Reservoir
375-36R	5774.3	2.17	33.1	Non-Reservoir
375-36R	5787.8	3.09	14.1	Non-Reservoir
375-36R	5788.9	1.08	25.8	Non-Reservoir
375-36R	5805.8	12.8	9.1	Sand
375-36R	5816.6	0.334	23.7	Non-Reservoir
375-36R	5833.2	2.24	18.9	Sand
375-36R	5834.3	4.59	21.2	Sand
375-36R	5853.9	0.0381	22.2	Non-Reservoir
375-36R	5858.4	0.0155	9.61	Non-Reservoir
375-36R	5861.2	0.00047	10.1	Non-Reservoir
387X-34S	6647.5	0.0216	5.9	Sand
387X-34S	6653.5	0.000676	10.7	Non-Reservoir
387X-34S	6656.4	0.0727	13.2	Non-Reservoir
387X-34S	6658.5	0.00471	13	Non-Reservoir
387X-34S	6660.5	0.123	12.7	Sand
387X-34S	6661.5	0.435	22.1	Non-Reservoir
387X-34S	6662.5	2	16.8	Sand
387X-34S	6668.5	0.362	11.8	Sand
387X-34S	6675.9	4.48	14.3	Non-Reservoir
387X-34S	6676.5	0.00014	2.17	Non-Reservoir
387X-34S	6677.5	0.0398	16.7	Non-Reservoir
387X-34S	6696.6	0.00482	11.3	Non-Reservoir
387X-34S	6706.5	11.3	18.2	Sand
387X-34S	6745.5	0.0805	17.7	Non-Reservoir
387X-34S	6788.5	0.0132	13.8	Non-Reservoir

Permeability and porosity for the Reef Ridge Shale in six wells from mercury injection capillary pressure data.

Well	Zone	Sample	Depth	Porosity (%)	Permeability (mD)
355X-30R	Reef Ridge	TEST1	5290	5.86%	0.00007
355X-30R	Reef Ridge	TEST2	5299.2	3.51%	0.00003
355X-30R	Reef Ridge	TEST3	5338.8	9.22%	0.00020
355X-30R	Reef Ridge	TEST4	5361.1	13.70%	0.09170
355X-30R	Reef Ridge	TEST5	5364.6	5.36%	0.00006
355X-30R	Reef Ridge	TEST6	5380.6	6.11%	0.00007
355X-30R	Reef Ridge	TEST7	5383.3	7.94%	0.00012
355X-30R	Reef Ridge	TEST8	5386.4	5.41%	0.00006
355X-30R	Reef Ridge	TEST9	5391.4	10.20%	0.00020
355X-30R	Reef Ridge	TEST10	5416.2	8.94%	0.00020
355X-30R	Reef Ridge	TEST11	5447.5	8.06%	0.00011
58A-25R	Reef Ridge	220	4419.5	22.90%	0.00410
58A-25R	Reef Ridge	239	4438.4	32.50%	0.00820
58A-25R	Reef Ridge	244	4443.4	31.80%	0.00730
58A-25R	Reef Ridge	270	4469.5	20.80%	0.00590
328-28R	Reef Ridge	1	5052.9	17.30%	0.00110
328-28R	Reef Ridge	2	5070.3	15.50%	0.00070
328-28R	Reef Ridge	3	5070.5	16.40%	0.00080
368H-19R	Reef Ridge	9	5020.5	22.00%	0.00340
368H-19R	Reef Ridge	10	5035.5	25.20%	0.00210
368H-19R	Reef Ridge	11	5042.5	23.80%	0.00160
365-24Z	Reef Ridge	7B	4154.6	13.60%	0.00030
365-24Z	Reef Ridge	8A	4160.5	16.30%	0.00039
365-24Z	Reef Ridge	9A	4162.5	10.80%	0.00019
365-24Z	Reef Ridge	16	4162	16.60%	0.00056
365-24Z	Reef Ridge	10C	4163.5	9.76%	0.00017
365-24Z	Reef Ridge	10B	4163.4	8.27%	0.00012
365-24Z	Reef Ridge	11A	4172.5	8.88%	0.00014
365-24Z	Reef Ridge	12A	4176.4	9.21%	0.00015
365-24Z	Reef Ridge	13A	4523.5	14.20%	0.00033
365-24Z	Reef Ridge	14B	4527.5	12.90%	0.00028
365-24Z	Reef Ridge	15A	4555.5	12.30%	0.00026
66-29R	Reef Ridge	225	4612.4	22.20%	0.00150
66-29R	Reef Ridge	230	4617.7	20.30%	0.00200
66-29R	Reef Ridge	256	4643.2	19.00%	0.08100
66-29R	Reef Ridge	267	4653.5	17.20%	0.04000
66-29R	Reef Ridge	269	4654.9	17.20%	0.06800
66-29R	Reef Ridge	283	4668.5	20.00%	0.00630
66-29R	Reef Ridge	289	4674	17.40%	0.03000
66-29R	Reef Ridge	291	4676.1	17.60%	0.00060
355X-30R	**Well Average**		**5369**	**7.7%**	**0.00018**
58A-25R	**Well Average**		**4443**	**27.0%**	**0.00617**
328-28R	**Well Average**		**5065**	**16.4%**	**0.00085**
368H-19R	**Well Average**		**5033**	**23.7%**	**0.00225**
365-24Z	**Well Average**		**4266**	**12.1%**	**0.00024**
66-29R	**Well Average**		**4650**	**18.9%**	**0.00965**
All Wells	**Average**		**4781**	**14.9%**	**0.00083**